

1 **Demographic history, linked selection, and recombination shape the genomic landscape of a broadly**
2 **distributed Pacific salmon.**

3

4 Quentin Rougemont^{1*}, Jean-Sébastien Moore¹, Thibault Leroy², Eric Normandeau¹, Eric B. Rondeau^{3,4}, Ruth
5 E. Withler⁵, Donald M. Van Doornik⁶, Penelope A. Crane⁷, Kerry A. Naish⁸, John Carlos Garza⁹ Terry D.
6 Beacham⁵, Ben F. Koop^{3,4}, Louis Bernatchez¹

7

8 ¹ Département de Biologie, Institut de Biologie Intégrative et des Systèmes (IBIS), Université Laval, Québec,
9 Québec, Canada QC G1V OA6

10 ² ISEM, Univ. Montpellier. CNRS, EPHE, IRD, Montpellier, France

11 ³ Centre for Biomedical Research, University of Victoria, Victoria, BC, Canada V8P 5C2

12 ⁴ Department of Biology, University of Victoria, Victoria, BC, Canada V8P 5C2

13 ⁵ Department of Fisheries and Ocean, Pacific Biological Station, 3190 Hammond Bay Road, Nanaimo,
14 British Columbia, Canada V9R 5K6

15 ⁶ National Oceanic and Atmospheric Administration, National Marine Fisheries Service, Northwest Fisheries
16 Science Center, Manchester Research Station, 7305 Beach Drive East, Port Orchard, Washington 98366,
17 USA

18 ⁷ Conservation Genetics Laboratory, U.S. Fish and Wildlife Service, 1011 E. Tudor Road, Anchorage, Alaska
19 99503

20 ⁸ School of Aquatic and Fishery Sciences, University of Washington, 1122 NE Boat Street, Box 355020,
21 Seattle, WA 98195 5020, USA

22 ⁹ Fisheries Ecology Division, Southwest Fisheries Science Center, National Marine Fisheries Service and
23 Institute of Marine Sciences, University of California–Santa Cruz, 110 McAllister Way, Santa Cruz,
24 California 95060

25

26 *Corresponding author e-mail: quentinrougemont@orange.fr (QR)

27 **Abstract**

28 Understanding the impacts of current human activities on within-species genetic variation requires a
29 thorough description of the historical factors that have shaped the genomic and geographical distribution of
30 nucleotide diversity. Past and current conditions influencing effective population size have important
31 evolutionary implications for the efficacy of selection, increased accumulation of deleterious mutations, and
32 loss of adaptive potential under the nearly neutral theory. Here, we gather extensive genome-wide data that
33 represent the extant diversity of the Coho salmon (*Oncorhynchus kisutch*) to address three issues. First, we
34 demonstrate that a single glacial refugium is the source of the majority of present-day genetic diversity, with
35 minor but detectable inputs from secondary micro-refugia. We propose a scenario whereby several ancestral
36 populations located south of the ice sheets expanded in postglacial time, swamping out most of the diversity
37 from other putative micro-refugia. Following this expansion, we identify particular populations having
38 undergone continuous declines in population size (N_e). Second, we combine multiple evidence from
39 demographic modelling, analysis of recombination landscape, and genome-wide landscape of diversity to
40 demonstrate that selection at linked sites and Hill-Robertson interference played a major role in shaping
41 genetic diversity across the Coho salmon genome. Third, we demonstrate that this demographic history
42 generated subtle differences in the load of deleterious mutations among populations, a finding that mirrors
43 recent results from human populations. Taken together, we found considerable support for the joint
44 contributions of demographic history and linked selection in the load of deleterious mutations. We suggest
45 that these inferences should be better integrated in conservation genetics of managed fish species which
46 currently focuses largely on within-population adaptation.

47

48 **Author Summary**

49 Reconstruction of a species' past demographic history from genome-wide data allows understanding how
50 historical factors interact with intrinsic genomic properties to shape the distribution of genetic diversity along
51 its genome and its geographic range. Here, we combine genotyping-by-sequencing and whole genome
52 sequence data with demographic modelling to address these issues in the Coho salmon, a Pacific salmon
53 species with rapidly declining census size in some parts of its range, notably in the south. Our demographic
54 reconstructions indicate a linear decrease in genetic diversity towards the north of the species range,
55 supporting the hypothesis of a major southern refugia for the Coho salmon and a northern route of
56 postglacial recolonization. Accordingly, the number of candidate deleterious homozygous derived mutations
57 was higher in northern populations. Demographic modelling also suggested the existence of cryptic refugia
58 that may have been missed with the use of simpler summary statistics. We further showed that the species'
59 genome was shaped by linked selection and biased gene conversion. In particular, local variation in
60 recombination rates have modulated the efficacy of natural selection. These processes, together with a
61 complex demographic history, can contribute to the load of deleterious mutations – an effect we argue should
62 be taken into account more routinely in conservation genetics studies.

63 Introduction

64 Both plant and animal biodiversity are currently declining or disappearing at unprecedented rates due to
65 human activity [1]. This leads to population size reduction, reduced genetic diversity, and to the sixth mass
66 extinction [2]. Before humans became major drivers of changes in species distributions and abundance,
67 long-term climate change had a major influence [3]. The Pleistocene glaciations resulted in major
68 contractions in the geographical distributions of many species into refugia that persisted in unglaciated areas
69 [4]. Postglacial range expansions often led to contacts between ancestral populations previously segregated
70 in different refugia [4,5]. The effects of long-term climate change combined with recent human-induced
71 population declines can foster genetic changes including a loss of genetic diversity, increased inbreeding,
72 increased load of deleterious mutations, and a loss of local adaptation [6].

73 In this context, it becomes important to understand how demographic history interacts with past and
74 ongoing selection and recombination to shape genetic variation. By disentangling past and current drivers of
75 range-wide genomic diversity, this information can inform management and conservation decisions [7].
76 Beyond conservation implications, such context provides a unique opportunity to address outstanding
77 questions in evolutionary biology. In particular, what is the role of gene flow in shaping heterogeneous
78 differentiation landscape during population divergence [8,9]? What are the demographic conditions required
79 to generate substantial differences in deleterious load among populations [10]?

80 A major challenge to understanding drivers of genome-wide patterns of diversity is that different
81 demographic processes can lead to similar contemporary genomic footprints [11]. As populations diverge,
82 they accumulate genetic incompatibilities forming barriers to gene flow [12], while the rest of the genome
83 may continue to be freely exchanged. As a consequence, the genomic landscape of divergence is expected to
84 vary, with greater differences between populations at genomic barriers as compared to genomic regions
85 exhibiting ongoing gene flow. However, similar patterns of heterogeneous genome-wide divergence can be
86 due to genetic hitchhiking of neutral alleles linked to selective sweeps [13] or to background selection (BGS;
87 [14]). These combined effects, referred to as linked selection reduces polymorphism at sites closely linked to
88 advantageous or deleterious variants, and therefore reduces local effective population size (N_e) along the
89 genome. The intensity of selection on linked loci will be mostly modulated by variation in local
90 recombination rate and by gene density [15,16]. Under linked selection, diversity (π , D_{XY}) and differentiation
91 (F_{ST}) metrics are expected to be positively and negatively correlated with genome-wide variation in
92 recombination rate (ρ) respectively, and with the density of targets (e.g., genes, regulatory regions) that are
93 subject to selection [14–18]. It is now increasingly recognized that neglecting BGS can bias demographic
94 inferences [19,20] or lead to false adaptive interpretations [21].

95 An understanding of historical demography is also essential for a sound interpretation of patterns of
96 deleterious mutation load observed among contemporary populations [10,22]. Population bottlenecks are
97 predicted to reduce potential for local adaptation, but also to reduce standing genetic variation and the
98 efficacy of selection [23,24]. In turn, a reduced efficacy of purifying selection leads to an increase in the
99 number of deleterious variants segregating in a population. Moreover, intrinsic genome properties, in
100 particular local variation in recombination rate or background selection, can favour the accumulation of

101 deleterious mutations [25]. From a conservation standpoint, populations harboring an elevated number of
102 deleterious variants might need to be monitored more closely.

103 Combining population genomics data with demographic modelling represents a powerful strategy to
104 test alternative hypotheses about historical drivers of existing genomic diversity. Previous studies employing
105 a similar approach have focussed mostly on species with a narrow geographic range, such as small islands
106 [26,27], which are on the verge of extinction [28–31] are strongly bottlenecked [32], shedding light on the
107 evolutionary consequences of small population size. Few studies, however, have investigated how historical
108 processes have shaped the geographical patterns in the distribution of genomic diversity in more broadly
109 distributed species, e.g., at the scale of a whole continent. An exception to this observation is the vast
110 literature on demographic reconstructions of human populations. Long-lasting debates in this literature
111 regarding the role of demography in generating mutation load differences among populations [22,33,34]
112 could benefit from studies of species displaying similarly complex demographic histories and broad
113 geographic distributions.

114 Salmonid fishes are economically important species that have suffered recent demographic declines
115 [35,36]. This is particularly the case for Coho salmon (*Oncorhynchus kisutch*), one of the five anadromous
116 species of Pacific salmon that supports important recreational and indigenous subsistence fisheries, which
117 has suffered dramatic population declines (> 90%) over the last three decades in parts of its range [36,37]. A
118 previous study investigated the range-wide population structure and demographic history of the species and
119 found a cline of decreasing diversity from south to north, as well as some endemic diversity in small putative
120 refugia [38] (see also [39]). This study indicated that Coho salmon may have survived the last glacial
121 maximum (LGM, i.e. the Fraser Glaciation in British Columbia, and the McConnell/McCauley Glaciation in
122 Yukon and Alaska; 23 to 18 Ky ago) in unglaciated areas of Haida Gwaii and Beringia in addition to areas
123 south of the ice sheets. This study, however, predates the genomic era and could not eliminate alternative
124 hypotheses regarding the origin and number of glacial refugia during the LGM. Most importantly, the
125 impacts of confounding factors such as background selection, recombination rate variation, and how these
126 factors may facilitate the accumulation of deleterious mutations could not be studied with the limited number
127 of genetic markers available at the time. In North America, the species is currently distributed from
128 California to Alaska [40]. Unglaciated areas that could potentially serve as glacial refugia persisted both
129 north (e.g. the Beringian refugium in Alaska, the Yukon Territory of Canada and areas of Asia and the Bering
130 Land Bridge) and south (e.g. all of the deglaciated area south of British Columbia, Canada) of the ice sheet
131 [40–42]. Other unglaciated areas (e.g. Haida Gwaii in British Columbia) could also have been micro-refugia
132 [43,44]. In this context, distinct demographic scenarios can be tested. Under a first scenario whereby
133 populations expanded north from a single southern refugium, we predict: *i*) a latitudinal decrease in genetic
134 diversity from south to north along with a pattern of IBD, and *ii*) ancestral populations located in areas south
135 of the ice sheets. Under a second scenario, populations expanded south from a single northern refugium, and
136 we predict the opposite geographic pattern. The third scenario corresponds to the survival of populations in
137 different refugia where we predict: *i*) the existence of clearly distinct genetic clusters, and *ii*) postglacial gene

138 flow with signatures of secondary contacts, with contact zones displaying higher genetic diversity through
139 postglacial admixture between different genomic backgrounds.

140 In order to test these alternative scenarios, we generated genome-wide data from nearly 2,000 Coho
141 salmon from California to Alaska, one of the most extensive genomic datasets for a non-model vertebrate
142 species to date. First, to resolve the species demographic history, we used a modelling approach that accounts
143 both for barriers to gene flow affecting migration locally, and for linked selection affecting the rate of drift.
144 Next, we tested the above predictions related to linked selection. Finally, we hypothesized that demographic
145 history and background selection shaped the pattern of deleterious mutation load, both within and among
146 populations. In particular, we hypothesized that postglacial re-colonisation influenced levels of standing
147 genetic variation and favoured the accumulation of deleterious mutations at the expansion front. In these
148 conditions, we predicted that genetic diversity should decrease as a function of the distance from the
149 ancestral populations, while the accumulation of putatively deleterious mutations should increase as a
150 function of the distance to the ancestral populations.

151

152 **Results**

153 *Overall genetic diversity and population structure*

154 A total of 1,957 individuals was sampled from California to Alaska representing 58 sampling locations
155 (mean $n = 34$ fish per location, Fig 1a, S1 Table) and genotyped using a genotype by sequencing (GBS)
156 method that generated 82,772 high quality filtered single nucleotide polymorphisms (SNPs). Another set of
157 55 individuals representing 11 sampling locations from the same range (Fig 1a), were whole genome
158 sequenced (WGS) to ~30X coverage, and used in specific analyses (S2 Table).

159 Levels of genetic diversity (observed and expected heterozygosity, π_{SNP}) were highest in formerly
160 deglaciated areas in the south (California, Cascadia, Fig 2a, Fig 1b) and decreased as a function of distance
161 from the southernmost site up to Alaska ($r = 0.64$, $p < 0.0001$, Fig 2a, S1 Fig). The Thompson River
162 watershed (Thompson R. hereafter) in southern British Columbia was an exception to this latitudinal pattern
163 and displayed the lowest average level of regional genetic diversity of all sampling locations which we
164 hypothesized to results from bottlenecks in this area. The remaining samples from British Columbia were
165 intermediate in genetic diversity.

166 The distribution of singletons provided further information regarding the most ancestral populations,
167 with older populations expected to have accumulated a higher density of singletons [45]. Counting the
168 number of singletons by sampling site and averaging by regional groups revealed the following differences:
169 Cascadian samples contained the highest number of singletons, with a mean of 1,263 singletons per site.
170 Californian samples had the fewest number of singletons ($n_{\text{MEAN}} = 55$) while Alaska harbored intermediate
171 density ($n_{\text{MEAN}} = 966$). Consistently, WGS data revealed 2.7 times more singletons in Cascadia (Tsoo-Yess
172 River) as compared to Alaska (Kwethluk River), whereas Thompson R. samples contained 6.7 times less
173 singletons, supporting the hypothesis of a pronounced bottleneck in these populations (S3 Table).
174 Similarly, the occurrence of private alleles was more prevalent among southern than northern populations,
175 being nearly twice as high in Cascadian ($n = 10,097$) than in Alaskan populations ($n = 5,270$). Again,

176 populations from the Thompson R. were an exception to this pattern with the lowest level of private
177 polymorphism ($n = 1,479$, S2 Fig).

178 Comparing the decay of linkage disequilibrium (LD) across populations based on the WGS data
179 indicated rapid LD decay across all samples (S3 Fig). The Thompson R. populations again departed from the
180 general pattern with a much reduced LD decay. Indeed, r^2 values decreased to 0.4 at approximately 342 kb
181 for Thompson R. whereas this r^2 value was attained between 13 and 34 kb for all other populations.

182 Next we used the β_{ST} coefficient to identify ancestral population [46]. Unlike F_{ST} estimates [47], this
183 index can account for the non-independence among populations and negative values are indicative of
184 ancestral populations [46]. Here, β_{ST} indicated that ancestral populations were located in previously
185 unglaciated areas corresponding to Cascadia ($n= 5$ localities), California ($n = 3$ localities) as well as one site
186 from southern British Columbia (Fig 2b, S4 Table). A linear decrease in β_{ST} as a function of distance from the
187 southernmost site was observed ($r = 0.60$, slope = $1.03e-04$, $p < 0.0001$) as expected under IBD. Support for
188 this IBD pattern was also observed using F_{ST} (S4 Fig, $r = 0.66$, slope = $4e-05$, $p < 0.0001$) as well as Mantel
189 tests ($r = 0.64$; $p < 0.0001$, $r = 0.72$; $p < 0.0001$ when removing Thompson R. populations). Average pairwise
190 F_{ST} across all populations was 0.095 and varied from 0.002 to 0.334 (S5 Fig), indicating moderate population
191 structure, typical of anadromous species connected by gene flow [48].

192 Model-based analysis of population structure failed to reveal a clear number of distinct populations
193 (K value). Instead, K values ranging from 30 to 60 all fit the data well (S6 Fig), due to the confounding
194 effect of IBD. The first axis of a Principal Components Analysis (PCA, Fig 3a) revealed a separation of the
195 sample from South to North with the most divergent samples found in California. The second axis revealed
196 the divergence from East to West but with a strong separation of the Thompson R. populations. Along these
197 axes populations followed an IBD pattern. These results were also supported by an MDS analysis (S7 Fig).
198 The third and fourth axis did not yield further information (S8 Fig).

199 We then used Treemix [49] to infer population splits and gene flow (Fig 3b). A first tree assuming no
200 migration (i.e. drift only) explained 98.1% of the variance observed. Adding up to four significant migration
201 events ($p < 0.0001$) explained over 99.1% of variance, then the proportion of explained variance plateaued
202 (S9 Fig). Populations from Cascadia occupied basal positions. California populations displayed pronounced
203 genetic drift, corroborating the high divergence observed in the PCA. Populations from Alaska (MSL River)
204 and Thompson R. also displayed higher genetic drift, in line with evidence based on analyses of genetic
205 diversity and genetic structure. The two most supported migration events occurred from Cascadia south to
206 California and north to the Thompson R. We note that populations followed the south to north arrangement,
207 with the samples from Cascadia displaying less drift than those further north.

208

209 *Demographic history*

210 In order to assess more formally the occurrence of one or more refugial origins for contemporary
211 populations, we performed the following explicit model-based inferences of population divergence scenarios
212 using $\partial a \partial i$ [50]. Our models account for the confounding effects of selection at linked sites and that of the
213 accumulation of local barriers to gene flow in the genome [19,51]. Four major demographic models were

214 statistically compared using groups identified in the PCA and with a focus on previously hypothesized
215 refugia (i.e., Cascadia, California, Haida Gwaii, Alaska). The following models were tested: strict isolation
216 (SI model), divergence with ancient migration (AM model), divergence with continuous gene flow (IM
217 model) and secondary contact (SC model; S10 Fig). A total of 69 pairwise comparisons was performed with
218 $\partial a\partial i$. In each pairwise comparison one single representative population from a putative refugium was
219 compared against one population from another refugium. Due to the high local structure within groups, we
220 avoided pooling samples into higher order groups (e.g., regional groups) as this would unavoidably bias our
221 results. Models incorporating linked selection and restricted introgression along the genome always received
222 highest support (S5 Table). ΔAIC (minimum value > 5) confidently discriminated models in 87% of the $\partial a\partial i$
223 comparisons (S5 Table). The SC model received the highest support in 46% of the comparisons, the AM
224 model in 30%, and the IM model in 14%, with 13% remaining unclassified. Scenarios including periods of
225 gene flow clearly outperform scenarios assuming no gene flow. The fact that secondary contact was the best-
226 supported model suggests that more than one glacial refugia contributed to the recolonization of the
227 contemporary range occupied by Coho salmon.

228 Assuming a generation time of 3.5 years [52] and mutation rate of $8e^{-9}$ bp/generation revealed
229 similar divergence time estimates among models (i.e., 57 Kya under SC, 40 Kya under IM, and 42 Kya under
230 AM, S6 Table). The median time of secondary contact (SC) was 10 Kya [min = 4,800 – max = 32,900],
231 corresponding roughly to the onset of the last glacial retreat (Fig 4A). Parameter estimates under the AM
232 model supported a very recent reduction in gene flow (mean < 1 Kya), which therefore represents a
233 demographic model similar to an IM model. Pronounced variation in effective population size (N_e) was
234 observed with the highest values in Cascadia populations (mean 12,800; range [3,500 – 16,500]). On
235 average, the smallest N_e were observed in the Thompson R. populations (mean 3,000; range [1,300 – 8,300],
236 Fig 4B), again consistent with a population bottleneck. However, smaller N_e values were also observed in
237 the isolated Navfac Creek population in Alaska ($N_e = 500$) and the Scott Creek population in California (N_e
238 = 1,800), which are the most divergent populations identified in the PCA. The McGarvey (California) and
239 Clackamas (Cascadia) populations identified as “ancestral” according to the β_{ST} displayed the highest N_e
240 (23,000 and 16,500). We also note that incorporating linked selection and barriers to gene flow further
241 reduced N_e , regardless of the model (S11 Fig). Intrinsic barriers to gene flow reduced the estimated
242 migration rate by half of its value and affected 20 to 40% of the genome (Fig 4C, S6 Table). Similarly, the
243 Hill-Robertson factor suggested that N_e was reduced to 37%-50% of its initial estimate and that
244 approximately half of the genome was affected (S6 Table).

245 We then investigated historical change in effective population size using the Sequentially Markovian
246 Coalescent in SMC++ [54] and the 55 whole genome sequences, which are representative of 11 populations
247 from California to Alaska (Fig 1, S2 Table). For ease of visualization, results for a subset of the populations
248 are presented in Fig 4D and details for all populations are displayed in S12 Fig. This analysis revealed: i) an
249 expansion of most populations approximately 12-20 KyA, concomitant with postglacial re-colonisation, ii) a
250 slow and steady decline in the Thompson R. (Fig 4D, S12 Fig), and iii) a split time between all pairwise
251 combinations of populations (median = 16,3 KyA, range = 6,7KyA - 61KyA, S13 Fig) compatible with the

252 onset of postglacial population expansion (Fig 4D) which was accompanied by an increase in N_e across
253 samples (Fig 4D). We note that using a different mutation rate (1,25e-8 mutations/bp/generations) yielded
254 estimates of split time that were more in line with the estimates of postglacial expansion (median = 9,6 KyA,
255 S13 Fig) and with less variance among compared population (min = 5 KyA – max = 18 KyA). Overall,
256 SMC++ results are consistent with previous analyses indicating that until recently, all populations shared a
257 similar demographic history. We caution against a strict interpretation of the most recent time. Indeed,
258 reliable estimates for present time require a high number of samples, whereas we only had five samples per
259 populations [54]. Similarly, exact N_e estimates should be interpreted cautiously and only the trend should be
260 considered rather than the exact values.

261

262 *Linked selection shape the Coho salmon genomic landscape*

263 We first described patterns of recombination and then tested correlations among genetic diversity (π),
264 divergence (D_{XY}), and differentiation (F_{ST}) parameters measured across the whole genome using 500 kb
265 sliding windows (Fig 5 A-C) and the population-scaled landscape of recombination (ρ) (Fig 5D) and gene
266 density (Fig 5E) to test our predictions using whole genome sequences.

267 This analysis first revealed a heterogeneous recombination landscape that varied both within and
268 among chromosomes. In particular, recombination rate was higher towards the ends of chromosomes (Fig
269 5D), as observed across many species [55] Second, we observed a negative correlation between
270 recombination rate and chromosome length ($R^2 = 0.481$, $p < 0.0001$, S14 Fig). To investigate the effects of
271 selection at linked sites, we summarised π (across all 11 WGS populations), D_{XY} and F_{ST} statistics (55
272 pairwise comparisons), using the first axis of a PCA (PC1) to obtain the common variation in these metrics
273 and reduce the dimensionality to single summary statistic (Fig 6, S15 Fig, S7 Table). PC1 captured 99% of
274 variance in π and in D_{XY} , indicating that the PC1 was effective at summarizing information about diversity
275 and divergence. All linear correlations among the tested variables were significant ($p < 0.0001$, S8A Table).
276 We found a positive correlation between PC1- π and recombination ($r = 0.54$, S8A Table) and a negative
277 correlation between PC1- π and gene density ($r = -0.20$) (Fig 6A-D). We also found a positive correlation
278 between PC1- D_{XY} and recombination ($r = 0.55$) and a negative correlation between PC1- D_{XY} and gene
279 density ($r = -0.21$). PC1- F_{ST} was negatively, albeit weakly correlated with both recombination ($r = -0.05$) and
280 gene density ($r = -0.04$, Fig 6B-E and C-F). We observed a correlation of 0.999 between π and D_{XY} , as
281 expected here because of a very recently shared common ancestor (Fig 6G). We also found a negative
282 relationship between PC1- π and PC1- F_{ST} ($r = -0.44$, Fig 6H) as well as between PC1- D_{XY} and PC1- F_{ST} ($r =$
283 -0.43 , Fig 6I). The smaller correlations between statistics involving F_{ST} can be explained by the modest
284 variance in F_{ST} explained by PC1 (37%).

285 In order to investigate further the effects of linked selection, we used mixed linear models that
286 integrate interactions among tested variables (i.e. recombination, gene density). These revealed a significant
287 effect of both recombination ($t = -41.17$, $p < 0.0001$, S8B Table) and gene density ($t = 5.72$, $p < 0.0001$) on
288 PC1- D_{XY} ($R^2 = 0.348$). The same was true when considering the correlation of PC1- π with recombination (R^2
289 $= 0.55$, Fig 6A-D, $t = -40$, $p < 0.0001$) and gene density ($t = 5.22$, $p < 0.0001$). Significant effects were also

290 found between PC1- F_{ST} and these variables (recombination: $t = 6.91$, $p < 0.0001$, gene density $t = 6.27$, p
291 $p < 0.0001$, interaction: $t = -4.073$, $p < 0.0001$, $R^2 = 0.025$, S8B Table). Similar correlations were found when
292 analysing populations separately (S9 Table). Therefore, our results suggest a role of linked selection in
293 shaping the patterns of diversity along the Coho salmon genome.

294 We then tested whether the efficacy of selection also played a role in shaping patterns of diversity
295 along the Coho salmon genome using the whole genome sequences. We measured ratios of non-synonymous
296 to synonymous polymorphisms (π_N/π_S) as a measure of the efficacy of natural selection and GC content at the
297 third codon position (GC3) as a proxy of local recombination rates. This metric was preferred as an indicator
298 of localized recombination rate variation at the gene scale, as opposed to the large population scale estimates
299 of recombination (ρ) over 250kb windows used above. Indeed, biased gene conversion (gBGC) occurs
300 because base mismatch during homologous recombination is known to be biased toward G and C
301 (conversion preferentially favours G+C over A+T bases) [56,57]. Here, we observed that the correlation
302 between GC3 and ρ ranged from $r = 0.3$ to 0.72 , depending on population. These modest correlations likely
303 reflect the loss of information about fine scale recombination rate variation when using 250kb sliding
304 windows, which also provides added justification to use the GC3 as a proxy. We found a strong correlation
305 between π_N/π_S and GC3 for all populations (Fig 7, linear models all $R^2 > 0.9$, $p < 0.0001$, S10 Table). Next,
306 we observed a negative correlation (linear model, $R^2 = 0.28$, $p = 0.051$) between historical N_e measured
307 before the onset of population expansion $\sim 13,000$ years ago and π_N/π_S ratio (S16 Fig), in agreement with the
308 nearly neutral theory of molecular evolution and indicating that our N_e estimates were good proxies of
309 genetic diversity. Second, among-population differences in π_N/π_S across all genes were modest (mean =
310 0.252), with a minimum value of 0.248 observed in Tsoo-Yess R. (Cascadia) and Robertson Creek (BC) and
311 maximum values of 0.257 and 0.256 observed in the Thompson R. and Inch Creek (BC) respectively. The π_N/π_S
312 differences among populations were more contrasted in areas of low recombination of the genome (Fig 7)
313 with lowest π_N/π_S values observed in the Kwethluk (Alaska, $\pi_N/\pi_S = 0.442$), Quilcene (BC, $\pi_N/\pi_S = 0.449$), and
314 Deschutes (Cascadia, $\pi_N/\pi_S = 0.451$) river populations. The highest values were observed in the Thompson
315 ($\pi_N/\pi_S = 0.551$), Klamath (California; $\pi_N/\pi_S = 0.543$) and Capilano (BC; $\pi_N/\pi_S = 0.495$) river populations.

316

317 *Spatial patterns of variation in deleterious mutations*

318 Given the complex demographic history of population size changes and spatial expansions leading to
319 secondary contacts in Coho salmon and the inference of linked selection, we predicted that deleterious
320 mutations should segregate at higher frequencies at the edge of the norther expansion front in Alaska, but
321 also in California likely representing a southern expansion from the Cascadian refugium, as well as in the
322 bottlenecked Thompson R. populations.

323 To do so, we tested for an increase in the derived allele frequency (DAF), and homozygosity of
324 predicted deleterious mutations at non-synonymous sites. We estimated derived alleles using whole genome
325 information from three outgroups: 1) Chinook salmon (*Oncorhynchus tshawytscha*) [58], 2) Rainbow trout
326 (*Oncorhynchus mykiss*) [59] and 3) Atlantic salmon (*Salmo salar*) [60]. Out of 4,427 non-synonymous
327 mutations identified with the GBS dataset from all 58 populations, PROVEAN (63) predicted a total of 1,297

328 deleterious mutations in at least one of these populations and for which we were able to identify the derived
329 allele. Deleterious mutations were maintained at lower DAF than synonymous variants (Wilcoxon-tests, all p
330 < 0.001). The DAF spectrum (Fig 8A) were computed for each major region (using a sample of size $n = 100$)
331 and for each population separately (S17 Fig). DAF were significantly different, among region (Kruskal-
332 Wallis chi-squared = 100.57, $df = 5$, p -value $< 2.2e-16$) as well as among population (Kruskal-Wallis chi-
333 squared = 638.59, $df = 57$, p -value $< 2.2e-16$, S11 Table). They showed that Alaska, Thompson R. and
334 California populations displayed more fixed deleterious mutations ($n = 18, 12$ and 11 respectively) than those
335 from the Cascadia region ($n = 3$). Haida Gwaii and BC populations were intermediate with 7 and 6 fixed
336 deleterious mutations respectively (Fig 8A). The three former regions also displayed higher frequencies of
337 polymorphic derived deleterious mutation (S18 Fig) compared to British Columbia or Cascadia (Wilcoxon
338 test, $p < 0.001$).

339 Next, we examined the count of homozygous (proportional to the load under a recessive model
340 [33,34]), heterozygous and of total derived deleterious mutations (proportional to the load under an additive
341 model [33,34]). In particular, we expected that mutations in a heterozygous state should be more frequent
342 than in a homozygous state, especially in populations with higher effective sizes, where selection should be
343 more effective at purging these mutations [23]. We found that 77% of deleterious mutations were maintained
344 in heterozygous states across all samples. Also, fish from Alaska, Haida Gwaii and California populations
345 harbored a significantly higher number of deleterious mutations in a homozygous state when compared to
346 Cascadia or British-Columbia (Wilcoxon-test, $p < 0.01$) (Fig 8B, S12 Table). When considering the total load
347 of derived deleterious mutations, we found that, on average, there were significantly more putatively
348 deleterious variants per individual in California, Cascadia, and Haida Gwaii populations than in fish from
349 Alaska, British-Columbia or the Thompson R. watershed (S12 and S13 Table, Fig 8C, Wilcoxon-test, $p <$
350 0.01), although these differences were modest. Finally, we tested the prediction that distance from the likely
351 ancestral source predicts the deleterious load, as observed in human populations [33]. We found a nearly
352 linear relationship between the distance from the putative origin of ancestral populations (the site with the
353 lowest β_{ST} in Cascadia) and the number of derived, homozygous, putatively deleterious mutations (HDD;
354 linear models, $p < 0.0001$; $R^2 = 0.13$, Fig 8D). Under the hypothesis that higher recombination rate leads to
355 more efficient purging of deleterious mutations we also expected deleterious mutations to be preferentially
356 located in areas of low recombination (S19 Fig). As expected, the GLM revealed that the occurrence of
357 deleterious mutations decreased as recombination rate increased ($\chi^2 = 4.90$, $DF = 1$, $p = 0.027$). This effect
358 was stronger when considering non-synonymous variants instead of putatively deleterious variants ($\chi^2 =$
359 10.07 , $DF = 1$, $p = 0.0015$). Given the negative correlation of recombination with chromosome length, we also
360 found a positive correlation ($r = 0.76$, $p < 0.0001$) between the chromosome length and the number of
361 deleterious variants by chromosomes, as expected when purging is more efficient in areas of higher
362 recombination (S20 Fig). To further examine this, we classified regions by recombination rate into high (ρ
363 > 4.516 , see methods), low ($\rho < 1.411$) and intermediate classes and found that there was a significant
364 excess of candidate deleterious mutations in areas of low recombination and depletion of candidate
365 deleterious mutations in areas of high recombination ($\chi^2 = 13.33$, $DF = 2$, $p = 0.0012$).

366 **Discussion**

367

368 Coho salmon is an emblematic fish species that has undergone population declines in recent decades
369 throughout its North American range. We generated one of the largest collections of GBS and WGS data to
370 date for a non-model vertebrate species, which revealed: *i*) a complex demographic history involving
371 population splits, gene flow, and secondary contacts; *ii*) linked selection and Hill-Robertson interference
372 shaped genetic diversity along the genome, and *iii*) this demographic history has resulted in modest yet
373 detectable differences in the frequency of deleterious variants across regions and populations, which also
374 varied as a function of recombination rate along the genome. Together, these observations help illuminating
375 the drivers of variation in genetic diversity throughout the genome of a broadly distributed species of
376 economic and cultural importance.

377

378 **Expansion from a major southern refugium and secondary contact with micro-refugia**

379 Our results revealed the existence of a major ancestral refugium located south of the ice sheets in Cascadia
380 (i.e., Washington and Oregon) where contemporary populations contain most of the genomic diversity
381 present over the entire North American range of the species. This conclusion was supported by observations
382 of: *i*) a pronounced south-north gradual decrease of genetic diversity, singleton density, and private
383 polymorphism, *ii*) a pattern of IBD, and *iii*) the occurrence of ancestral populations south of formerly
384 glaciated areas. Therefore, although the so-called Beringian refugium that persisted north of the ice sheet
385 (mainly comprising Alaska and the Yukon Territory) was important for many temperate species (6), this was
386 not the case for Coho salmon. The gradual northward decrease in diversity also suggests that populations
387 subsequently expanded from Cascadia to British-Columbia and Alaska [4,5] and is indicative of a serial
388 founder effects due to small proportions of individuals issued from ancestral populations colonising new
389 locations, a process amply documented in humans (e.g., [61]). This expansion was likely postglacial,
390 although GBS-based parameter estimates of divergence time under AM, IM, and SC (~ 30 to ~ 45 KyA)
391 were not in full agreement with SMC++ estimates using WGS (~18 KyA). This, however, is expected given
392 the different assumptions made by the various models compared and that gene flow is expected to delay
393 divergence [62]. The last glacial period (Wisconsin Glaciation) which lasted from ~ 120 Ky to ~11 KyA was
394 interrupted by an interglacial period from 55 to 25 KyA ([40]). Therefore, our results indicate that neither
395 Beringia nor Haida Gwaii were refugia before the onset of the Wisconsin Glaciation. However, it is possible
396 that individuals from Cascadia already colonized and subsequently diverged in Alaska (Beringia) 55 to 25
397 KyA. If this was the case, however, the contribution of Beringia is likely minor as no strong footprint of
398 ancestral diversity and no signal of secondary contact was inferred in this area.

399 While a single major southern refugium hypothesis is well supported by our data, our analyses also
400 revealed patterns consistent with minor contributions of micro-refugia on extent genomic diversity. Indeed,
401 our demographic modelling supported a model of postglacial (10-20 KyA, S6 Table) secondary contact (SC)
402 detected in several pairwise comparisons among populations between California and Haida Gwaii ($n = 10$
403 pairwise comparisons), Cascadia and Haida Gwaii ($n = 2$), California and Thompson R. ($n = 11$), and

404 between Cascadia and Thompson R. ($n = 1$). These results are counter-intuitive, because contacts between
405 northern sites and California, but bypassing Cascadia, seem unlikely. A possible explanation is that our
406 statistical power to detect SC involving putative micro-refugia was reduced. Here, indeed, the SC period
407 represented a large proportion (22% on average) of the total divergence time across all models. However,
408 models of SC can easily be confounded with models of isolation with migration when SC represents a large
409 period of time ($> 10\%$) relative to the total period of divergence, as observed in our investigations [19,63].
410 Still, our inference of SC supports the hypothesis that smaller micro-refugia have persisted along the Pacific
411 Coast [43,64]. In particular, the Haida Gwaii archipelago is known for high endemism, and its role as a
412 refugium for mammals, invertebrates, and angiosperms is well established [64–66]. The divergence time
413 inferred between populations from California and Haida Gwaii was relatively recent (39 KyA), in the range
414 of inferred divergence times for bird species from the region [67] and in the time frame of the last
415 interglacial period 55 to 25 KyA. Our results also indicated a pronounced divergence between California and
416 Cascadia, suggesting that these were likely two separated refugia, thus supporting the hypothesis of “refugia
417 within refugia” [43,67]. However, California populations have suffered from strong census size reductions in
418 recent decades [68], possibly increasing genetic structure and lowering effective population size. Given our
419 estimates of split times and population sizes, the possible refugium in Haida Gwaii, and California were
420 demographically small and relatively recent, such that populations in these areas were unlikely to have
421 accumulated significant endemic genetic diversity. The case of the Thompson River, on the other hand, is
422 rather intriguing as this region was entirely covered by ice during the Pleistocene. A possible explanation is
423 that a strong and continuous bottleneck has led to a false signal of SC. The SC was the most parameterized
424 model and was therefore more likely to be falsely supported. A model including more drastic and continuous
425 post-divergence changes in population size may fit the data well but would likely be difficult to statistically
426 separate from a model of secondary contact. British-Columbia populations, located at intermediate latitudes,
427 also displayed intermediate levels of genetic diversity, with some populations displaying similar or higher
428 diversity than those located in Cascadia, further supporting the hypothesis of post-colonization admixture
429 between different refugia [69] Complex history of divergence in different refugia and possible mixing was
430 also inferred in the Chinook salmon along the Pacific Coast and was associated to different migratory
431 ecotypes [70]. A potential limitations of our current approach is that we did not incorporate samples from
432 Asia, where the Coho salmon also occurs [41]. Whether this would change our inferences remains an open
433 question. In summary, our modelling approach revealed the presence of multiple cryptic refugia that would
434 otherwise have been missed because their endemic genetic diversity appears to have been largely wiped out
435 by a major demographic expansion out-of-Cascadia, which has clearly been the primary contributor of extent
436 genomic diversity in North American Coho salmon. Knowledge of this non-equilibrium demography will
437 important to help interpret adaptive and deleterious genomics landscape in future studies.

438

439 **Selection at linked sites shape genome wide variation**

440 We also explored the role of gene flow and linked selection in generating a heterogeneous differentiation
441 landscape along the genome, a hotly debated topic in evolutionary genomics [8,9,71,72]. Disentangling the

442 two processes is of fundamental importance for correctly interpreting the origin of genomic islands of
443 divergence and genome scan results [73,74]. Although a positive relationship between absolute and relative
444 divergence may reveal the presence of barriers to gene flow [9], this is not relevant for early stages of
445 divergence [75], as in the present study. Instead, our modelling approach best supported a role of both gene
446 flow and linked selection. In particular, the role of linked selection is supported by the positive correlations
447 between π or D_{XY} and recombination rate, while F_{ST} was negatively correlated with recombination rate
448 [73,75]. The negative correlations between π or D_{XY} and gene density provided further evidence for the role
449 of linked selection [17]. Here, heterogeneous genomic divergence did not arise after speciation, as suggested
450 by Cruickshank & Hahn [9]. Instead, our within-lineage study indicated that linked selection arose within
451 structured populations, in line with recent findings in birds [73]. Similar effects of linked selection were
452 suggested between the more diverged ancestral lineages within Atlantic salmon (>1 MyA) [76]. Given that
453 correlated genomic landscapes have been reported among species diverged for over tens of millions of years
454 [77,78], it would be interesting to investigate how linked selection has also shaped genomic landscapes
455 within the entire radiation of salmonid fishes. Indeed, salmonid species have undergone a whole genome
456 duplication approximately 90 MyA [79] affecting recombination throughout their genome [57,80,81]. Precise
457 mapping of the genomic locations of duplicated regions will allow an improved understanding of how
458 recombination rate varies in these regions although we do not expect that will affect our main conclusion
459 related to linked selection. Salmonid genomes are also characterised by pronounced male heterochiasmy
460 [82,83] and here, we observed a significant correlation between recombination and chromosome length,
461 indicative of crossover interference [84]. Both heterochiasmy and crossover interference contribute to
462 heterogeneity in recombination rates and likely favour the effect of linked selection. Given that most non-
463 neutral mutations are deleterious [85], and given the impact of recombination across the genomes of fishes,
464 models of background selection could be the null model against which to test adaptive hypotheses [21]. Our
465 data revealed that the GC3 was a good proxy of recombination and that it was strikingly well correlated with
466 our proxy for the efficacy of natural selection (π_N/π_S). As expected, this metric revealed differences in the
467 most bottlenecked populations from the Thompson River drainage, where the severity of the bottleneck
468 mimics the effect of domestication bottleneck (e.g. [86]). Indeed, the Thompson R. populations displayed a
469 higher burden of non-synonymous mutations, and we suggest that the strong bottlenecks in these populations
470 had a dramatic impact on the efficacy of natural selection. When considering only genomic regions of low
471 recombination, however, we also found that some California populations also displayed an increased π_N/π_S
472 ratio. Given that these populations have recently undergone large declines in abundance [68], we expected a
473 lower efficacy of purifying selection in regions of low recombination where Hill-Robertson interference
474 should be high [82]. Furthermore, we suggest that the severe and recent demographic declines documented in
475 California populations compared to more long term and putatively less severe declines in the Thompson R.
476 may explain why differences were detected only in genomic regions of low recombination in the former but
477 genome-wide in the latter. Regardless, the non-equilibrium demography, and role of linked selection, in
478 particular background selection, are predicted to favour the accumulation of deleterious mutations, an
479 important finding to manage declining species.

480 **Accumulation of deleterious mutations under complex demography**

481 In the literature, contradictory results have been reported regarding the role of demographic history on the
482 load of deleterious mutations [10,33]. On the one hand, processes such as strong and repeated bottlenecks
483 [24,32], including domestication [86,88], large expansions [89,90] or postglacial colonization [91] can all
484 increase the deleterious load. On the other hand, empirical studies in human indicate that recent demography
485 should not have a strong impact on the load of deleterious variants over the long term [10]. However, other
486 studies indicate that strongly deleterious variants affecting fitness can still display increased in frequency due
487 to demographic growth [10]. Here, the inferred demographic history, together with support for linked
488 selection and gBGC, provides ideal conditions to favour the accumulation of deleterious mutations. In
489 particular, we found that populations displaying smaller effective population size (e.g. California), and those
490 at the extreme of the expansion front (Alaska), displayed deleterious mutations at higher derived allele
491 frequencies, and more frequently in homozygous state, in line with the nearly neutral theory. Similar findings
492 have been observed in domesticated species [86] and recently in Isle Royale wolves [26] where decreased
493 population sizes and inbreeding increased the frequency of deleterious recessive mutations. Overall, these
494 results are consistent with recent empirical findings in which small populations or populations at the
495 expansion front carry more homozygous derived deleterious mutations [26,27,86]. These deleterious
496 mutations in homozygous state are expected to be purged by purifying selection [23,92]. Populations from
497 Cascadia, with higher effective population sizes, contain a higher number of putatively deleterious variants
498 in heterozygous state, as expected from population genetics theory. We also found a nearly linear relationship
499 between the number of derived deleterious mutations in homozygous states and geographic distance from the
500 putative refugial source in Cascadia. This relationship mirrors the findings pertaining to the ‘out-of-Africa’
501 expansion of human populations [33], although the maximum geographic distance in our study is an order of
502 magnitude smaller than in the human studies, and that the presence of multiple refugia (as opposed to the
503 sole African ancestral origin for humans) may have contributed to obscure somewhat the relationship.
504 Moreover, pronounced genetic drift or bottlenecks observed in some populations (e.g. Thompson R. and
505 California) may have contributed to reduce the efficacy of selection [24]. Finally, the lower prevalence of
506 deleterious mutation in fish from British-Columbia might also be explained by post-glacial admixture. In
507 some small populations it is possible that these mutation initially reached fixation but subsequently became
508 masked in heterozygous state due to gene-flow and introgression [93]. Similar effect could be due to
509 artificial supplementation programs, but the origin of source populations and intensity of stocking in our
510 study populations are poorly documented. Finally, we observed that recombination was significantly
511 correlated with the proportion of non-synonymous mutations and with the load of deleterious mutations, with
512 more deleterious mutations being found in genomic regions of low recombination. This is in line with
513 theoretical predictions (e.g. Hill-Robertson Interference discussed above), and also empirical studies in other
514 species [94,95]. Overall, our results suggest that Coho salmon populations with highly reduced population
515 sizes are exposed to higher inbreeding depression – a prediction with major conservation implications and
516 which should be investigated further in future studies.

517 **Conclusion**

518 In this study, we presented a rare combined assessment of the relative role of complex demographic history
519 (investigated both by empirical genomic data and modelling) and intrinsic genomic factors (recombination,
520 linked selection) in shaping drivers of the genomic landscape of a broadly distributed species. Complex
521 demographic processes including population expansion, isolation, and secondary contact were revealed
522 through the use of an extensive modelling framework. Moreover, our results highlighted the necessity of
523 accounting for local variation in recombination rate, a key driver of linked selection. Altogether, these
524 processes influence the efficacy of selection and can favour the accumulation of mutations affecting fitness.
525 Our findings suggest that such approaches offer enormous potential in the field of conservation genomics to
526 disentangle the impacts of historical vs. recent drivers of demographic declines and for assessing the
527 distribution of not only putatively beneficial, but also deleterious variants. We propose that future studies
528 should also integrate in-depth analysis of selective sweeps which will be necessary to investigate into more
529 details how linked selection, through background selection and hitchhiking, acts to maintain deleterious
530 mutations in the genome [96]. Finally, while it has become routine with new genome-wide datasets to focus
531 on the effect of positive selection and documenting patterns of local adaptation [7], this focus ignores the
532 fundamental prediction that most new mutations are likely to be deleterious [85]. An increased focus on
533 deleterious mutations would provide a more nuanced view of genomic evolution in wild species which
534 would benefit both the fields of evolutionary and conservation genetics

535

536 **Methods**

537 ***Genotyping By Sequencing***

538 A total of 2,088 individuals was collected from 58 sample sites located along the Pacific coast from
539 California to Alaska (S1 Table and Figure 1). DNA was extracted from all individuals and sequenced using a
540 GBS method (protocol detailed in [97]). Reads were aligned to the Coho salmon reference genome v1
541 (GCF_002021745.1) using bwa-mem 0.7.13 [102]. Samtools v1.7 was used to keep reads with a
542 mapping quality above 20, remove supplementary alignment and unmapped read. Variants were then
543 called with Stacks v1.46 [98]. To do so, the module “pstacks” was used with a minimum depth of 5, and up
544 to three mismatches were allowed in catalog assembly. The module “populations” was run to produce a vcf
545 file that was filtered with a custom python script. We performed stringent filtering to remove SNPs that were
546 1) genotyped in less than 60% of the individuals; 2) at a mean depth of sequencing below 7, and 3) with
547 observed heterozygosity above 0.60, thus resulting in 93,000 SNPs. The pipeline for SNP calling is available
548 on github at https://github.com/enormandeu/stacks_workflow/releases/tag/coho_demography_paper. Next,
549 we removed any individuals with more than 5% missing data and finally only kept SNPs present in at least
550 95% of the individuals yielding a total of 82,772 filtered SNPs for 1,957 individuals. Remaining filtration
551 was done according to the requirement of each analysis performed below.

552 ***Genetic diversity and ancestral populations***

553 For each sampling location we estimated the observed heterozygosity and π using vcftools 0.1.16 [99] and
554 hierfstat [100]. The most likely ancestral populations were identified using β_{ST} [46]. A total of 1,000
555 bootstraps was performed to obtain the 95% confidence intervals around the β_{ST} . Weir and Cockerham's F_{ST}
556 estimator θ [47] was computed in vcftools. We measured the relationship between observed heterozygosity,
557 β_{ST} , F_{ST} and the distance to the southernmost site using linear models. We also verified the relationship
558 between F_{ST} and the distance to the southernmost site using Mantel tests with 10,000 permutations. Vcftools
559 was also used to identify singletons (i.e. variants present in one single individual across the whole dataset).
560 Their distributions were then summed in each locality. We then computed the averaged (min, max and
561 median) number of singletons at the regional level. The scripts are available on github at [https://github.com/](https://github.com/QuentinRougemont/utility_scripts)
562 [QuentinRougemont/utility_scripts](https://github.com/QuentinRougemont/utility_scripts)

563

564 ***Population structure, admixture and gene flow***

565 Levels of ancestry and admixture proportions were inferred with the snmf function implemented in the R
566 package LEA [101]. We allowed less than 5% of missing data. We then kept a set of SNPs in approximate
567 linkage equilibrium by removing pairs of variants with r^2 greater than 0.2 (option --indep-pairwise 50 10 0.2)
568 resulting in 40,632 SNPs. K-values ranging between 1 and 60 were tested and cross-validations were
569 obtained using the cross-entropy criterion with 5% of masked genotypes. The default value for the
570 regularization parameter was used to avoid forcing individuals into groups and hence underestimating
571 admixture. Similar results were obtained from Admixture [102] and are not presented here. Genetic
572 relationship among all salmon was assessed using a PCA with the R package ade4 [103] based on the LD-
573 pruned dataset (40,632 SNPs). We used a 1% minor allele frequency (MAF) threshold and allowed less than
574 4% missing data. Formal tests of admixture were performed using Treemix [49] using the LD-pruned dataset
575 of 40,632 SNPs and without any MAF threshold. A MDS was also constructed using plink and plotted with
576 the ggplot2 [105] R package. We ran Treemix allowing up to 20 migration events and performed 500
577 bootstraps replicates of the best model to obtain robustness of the nodes. The “best” model was inferred after
578 inspecting the relevant migration edges by measuring the percentage of variance explained as migration edge
579 were added to the tree as well as by assessing the p-value associated to each migration edge. A total 500
580 bootstraps replicate was performed under the “best” model and under a model without migration to infer the
581 robustness of the nodes. The scripts are available on github at
582 https://github.com/QuentinRougemont/treemix_workflow

583

584 ***Explicit demographic inferences.***

585 We tested alternative hypotheses of secondary contact between major regional groups (Haida Gwaii,
586 California, Cascadia (Washington-Oregon), Alaska, British Columbia, Thompson R.) of populations by
587 comparing alternative divergence scenarios represent in Fig S12 and initially described in [19,76].
588 Alternative hypotheses of secondary contacts were tested between major groups by testing the significance
589 of alternative divergence scenarios. The four major models tested included a model of Secondary Contact

590 (SC), a model of Strict Isolation (SI), a model of Ancient Migration (AM) and a model of Isolation with
591 Migration (IM).

592 The models shared the following parameters: the ancestral populations of size N_{anc} , splits at time T_{split}
593 into two daughter populations of size N_1 and N_2 . Under the SI model, no gene flow occurs between the two
594 populations. Under AM, gene flow occurred between T_{split} and T_{am} and is followed by a period of strict
595 isolation. Under IM, gene flow occurs at a constant rate at each generation between the two populations.
596 Gene flow can be asymmetric, so that two independent migration rates m_{12} (from population 2 to 1) and m_{21}
597 (from population 1 to 2) were modeled. Under the SC model, the population evolved in strict isolation
598 between T_{split} and until T_{sc} where a secondary contact occurs continuously up to present time. Gene flow is
599 modeled as $M = 2N_{ref}m$. In $\partial a \partial i$, heterogeneous introgression was modeled using two categories of loci
600 occurring in proportions P (i.e., loci with a migration rates M_{12} and M_{21}) and $1-P$ (i.e., loci with a reduced
601 effective migration rates Me_{12} and Me_{21}) across the genome. The same procedure was used to account for
602 linked selection by defining two categories of loci with varying effective population sizes (proportion Q of
603 loci with a “neutral N_e ” and a proportion $1-Q$ of loci with a reduced effective population size due to either
604 linked or background selection). To quantify how linked selection affects reduced N_e , we used a Hill-
605 Robertson scaling factor (Hrf) to relate the effective population size of loci influenced by selection ($N_r = Hrf$
606 $\cdot N_e$) to that of neutral loci (N_e).

607 Models were fitted using the diffusion theory implemented in $\partial a \partial i$ [50] and also includes the effect of linked
608 selection and barriers to gene flow as detailed in [19,104]. $\partial a \partial i$ uses the SFS as a summary of the data. For a
609 given demographic model, the SFS is computed using diffusion approximation and compared to the
610 empirical SFS using AIC. Here, we started from the whole file containing 200,000 SNPs and used one single
611 SNP per GBS locus, filtered the data to minimize missing data. No MAF was used and singletons were kept
612 to obtain ascertainment-free estimates of demographic parameters. Ideally, no Hardy-Weinberg Equilibrium
613 (HWE) filter should be used for demographic inferences, as this also biases the distribution of allele
614 frequencies. However, to remove paralogs present in the Coho salmon genome, a permissive HWE filter
615 based on a p-value of 0.0001 was used. Here, a total of 69 pairwise comparisons between populations from
616 the major regional groups was performed in order to test for a prevailing pattern. Here, the regional groups
617 considered were all previously unglaciated areas during the LGM, namely California, Cascadia, Alaska
618 (although some samples were likely under ice at different time periods) and Haida Gwaii. For each model, 20
619 independent replicate runs were performed and only models with the lowest AIC and ΔAIC were kept. A
620 model was classified as “ambiguous” and not used for parameter estimation if ΔAIC between the best model
621 and second-best model was below 10. The whole pipeline is available at
622 <https://github.com/QuentinRougemont/DemographicInference>.

623

624 ***Analyses based on whole genome resequencing data.***

625 We used 55 individuals representing 11 populations from California to Alaska (S2 Table). Each individual
626 was sequenced on an Illumina platform using paired-end 150 bp reads. Reads were processed using fastp for
627 trimming [105], bwa mem v0.7.13 [106] for mapping, samtools v1.7 requiring a minimum quality of 10, and

628 picard to remove duplicates (<http://broadinstitute.github.io/picard/>). Then SNP calling was performed using
629 GATK [107]. Genotypes were filtered for depth between 10 and 100 reads to remove low confidence
630 genotypes including potential paralogs, displaying high coverage. Then following GATK Best Practices we
631 excluded all sites that did not match the following criterion: $MQ < 30$, $QD < 2$, $FS > 60$, $MQRankSum < -20$,
632 $ReadPosRankSum < 10$, $ReadPosRankSum > 10$. We also generated a vcf file using the samtools mpileup
633 pipeline, merging individuals with bcftools and performing the same stringent filtering as with the vcf
634 constructed with GATK. Finally, we also generated a separate vcf file using the emit-all-site option to call
635 variable and invariable sites across the whole genome. This vcf file was used in the sliding windows analysis
636 below to test the effect of linked selection. The whole pipeline is available on github
637 (https://github.com/QuentinRougemont/gatk_haplotype).

638 SMC++ [53] was used to infer changes in population size through time. SMC++ works similarly to
639 the PSMC model but takes advantage of information contained in the Site Frequency Spectrum (SFS) in
640 addition to linkage disequilibrium, and is particularly well suited to analyse large sample sizes. Estimates of
641 population size changes were performed for all 11 populations. Splitting time was estimated between all
642 pairs of samples based on the joint SFS. A generation time of 3.5 years and a mutation rate of $8e^{-9}$
643 mutation/bp/generation were applied. The pipeline to reproduce the analysis is available on github
644 (https://github.com/QuentinRougemont/smcpp_input)

645 We computed pairwise linkage disequilibrium using vcftools with the r^2 statistics calculated in all 11
646 populations separately. A window of 1,000,000 base pairs was used and all SNPs were included. To reduce
647 the number of SNPs, we allowed no missing data and used a MAF of 10% and a p-value of Hardy-Weinberg
648 disequilibrium of 0.05 in each population, keeping between 2 and 4 million SNPs depending on the
649 population. We then estimated LD decay by plotting LD against physical distance measured in base pairs and
650 using smoothing functions implemented in ggplot2 [108] package in R. vcftools was also used to identify
651 singletons, for which the distribution were counted by localities, as for the GBS dataset.

652 We used LDHAT software [109] to estimate effective recombination rates ($\rho=4.Ne.r$ where r
653 represents the recombination rate per generation and Ne is the effective population size) along the genome.
654 Unphased genotypes were converted into LDHAT format using vcftools with a minimum MAF of 10% since
655 only common variants are useful for such inferences [109]. Following the authors' guidelines, the genome
656 was split in chunks of 2,000 SNPs with overlapping windows of 500 SNPs to compute recombination rate
657 and data were then merged together. We measured recombination rates for each river as well as globally
658 including all populations except the population from the Thompson R. watershed that was too divergent from
659 the remaining samples. The pipeline to reproduce the analysis is available on github
660 (https://github.com/QuentinRougemont/LDhat_workflow).

661

662 ***Clarifying the role of linked selection***

663 The genetic landscape of divergence was measured by estimating levels of nucleotide diversity (π), gene
664 density, levels of genetic differentiation (F_{ST}), levels of divergence (D_{xy}), and scaled recombination rate
665 along the genome. Estimates of π , F_{ST} , and D_{xy} were computed into 500kb windows using Python scripts

666 available from [110]. Gene density was computed directly from the gff file of the Coho salmon genome v1.0
667 (NCBI ftp file: ftp://ftp-trace.ncbi.nih.gov/genomes/Oncorhynchus_kisutch/GFF/; Rondeau et al. In prep)
668 and measured in 500 kb windows. Recombination rates were averaged into 250 and 500-kb windows using a
669 Python script after being estimated with LDhat as described above. We used a PCA to obtain a synthetic
670 view across all 11 π estimates, and all pairwise 55 Dxy and 55 F_{ST} separately. This allowed capturing the
671 common variation affecting these three estimates. First, simple Spearman correlations based on linear models
672 testing each (z-transformed) variable projected on the PC1 axis separately were carried out to produce fig 5.
673 Then Mixed Linear Models were used to test for correlations between either π , Dxy, or F_{ST} and either
674 recombination landscape (ρ) or gene density windows as explanatory variables, with and without
675 interaction. Correlations were also calculated considering each π , Dxy, and F_{ST} by population separately
676 without PCA transformation (S9 Table) which returned patterns that were congruent with those observed
677 with PCA results.

678

679 **Measuring GC content, Non-Synonymous and Synonymous diversity**

680 The pipeline developed by [111] was used to compute Tajima's π estimator of nucleotide diversity and the
681 GC content over non-overlapping 10-kb windows. Then we concatenated the gene into different classes
682 according to their length and compute π_N and π_S over 4 mb windows, which allows circumventing the
683 problem associated to low π_S values. We then verified the correlation between populations scaled
684 recombination rate (ρ), measured over 250-kb windows and GC at the third codon position (approximately
685 neutral). To do so, we assigned a ρ value for each gene according to its position into each 250-kb windows.
686 Then we averaged ρ values over the same length class as GC3 classes and compared the median population
687 recombination rate estimates and GC3s over 4-mb windows. Finally, we measured the correlation between
688 GC3s and π_N/π_S using linear models.

689

690 **Genetic load estimation from the GBS data set**

691 *Estimating ancestral and derived alleles*

692 We used the derived allele count as an estimator of deleterious allele count. We used the genomes of three
693 outgroup species, the chinook salmon, the rainbow trout, and the Atlantic salmon, to classify SNPs as
694 ancestral or derived. Whole genome data for the chinook salmon ($n = 3$ individuals) were provided by one of
695 us (B. Koop, unpublished), whereas rainbow trout ($n = 5$) and Atlantic salmon ($n = 5$) data were downloaded
696 from NCBI Sequence Read Archive (rainbow trout, SRA, Bioproject : SRP117091; *Salmo salar* SRA
697 Bioproject: SRP059652). Each individual was aligned against the Coho salmon V1 reference genome
698 (GCF_002021745.1) using GATK UnifiedGenotyper and calling every SNP using the EMIT_ALL_SITES
699 modes. We then constructed a Python script and determined the ancestral state of the GBS SNPs if 1) the
700 SNP was homozygous in at least two of the three outgroups, and 2) match one of the two alleles identified in
701 Coho salmon. Otherwise, the site was inferred as missing and not used in subsequent analyses.

702 *Measuring damaging impact of non-synonymous alleles*

703 We tested differences in mutation load among populations as follows. The software Provean [112] was used
704 to predict whether a given non-synonymous mutation was deleterious with a threshold score of -2.5 or less
705 using the pipeline available at https://github.com/QuentinRougemont/gbs_synonymy_with_genome. We
706 analysed data in two ways: first we counted the total number of putative homozygous deleterious alleles per
707 individual as well as the total number of deleterious alleles (both in homozygous and heterozygous states)
708 using: $N_{total} = 2 \times N_{homo} + N_{hetero}$ [34]. These individual values were then averaged per population and major
709 regional groups (i.e., California, Cascadia, British Columbia, Haida Gwaii, Thompson, and Alaska). We then
710 computed derived allele frequencies (DAF) in all sampling locations and across mutation categories
711 (synonymous, non-synonymous, and non-synonymous deleterious) and tested for significant allele frequency
712 differences among populations in non-synonymous and non-synonymous deleterious mutations using
713 Wilcoxon rank sum tests. DAF spectra were constructed for all population separately. For the ease of
714 visualisation, we also constructed DAF spectra by region for a sample of size $n = 100$ individuals (Fig 7A).
715 This size was chosen according to the smallest sample size of the three combined Haida Gwaii populations.
716 Finally, we tested for a preferential enrichment of “hotspots or coldspots” of recombination in deleterious
717 mutations. To define a coldspot, we first computed a lower bound that we defined as the $mean_{RHO} -$
718 $5 \times \text{standard errors}$ for each chromosome separately. Similarly, “hotspots” of recombination were identified
719 using an upper bound defined as $mean_{RHO} + 5 \text{ standard errors}$. We then tested if the average recombination rate
720 of each of the 250 kb windows was falling below the threshold (for coldspot) or above it (for hotspots). We
721 then tested if recombination hotspots and coldspots contained more or less putatively deleterious mutations
722 than “normally” recombining regions using χ^2 tests. Linear mixed effects models were further used to test if
723 there was a relationship between recombination rate and the distribution of putatively deleterious mutations.
724 The response variable was the deleterious state considered binomial (0 = non deleterious, 1 = deleterious)
725 and the explanatory variable was the recombination rate. The chromosome identity was included as a random
726 effect. This model was compared against a null model excluding recombination rate. The analysis was
727 replicated but using the synonymous and non-synonymous state as the response variable instead of the
728 putatively deleterious state of the considered mutation. Models were carried out in R using the LME4
729 package [113]. Finally, we used SnpEff v3.4 [114] to obtain the functional annotations of the putatively
730 deleterious variants. The annotations were comprised of mis-sense variants, non-coding transcripts, 3' and 5'
731 untranslated regions, 5kb up- and down-stream variants, intergenic and intronic, splice acceptor and splice
732 region, stop gained and start loss (S14 Table). We found 35% of deleterious mutations to be missense
733 variants, 38% to be non-coding transcript and 22% to be either upstream or downstream gene variants, with
734 the remaining being spread over the categories.

735 **Ethic Statement**

736 A permit number SIRUL 111722 was obtained to work on DNA sequences.

737

738 Raw data will be deposit on NCBI together with Short Read Archive (SRA) accession number.

739 **Acknowledgements:**

740 We thank B. Bougas, A. Perrault-Payette, C. Hernandez for laboratory support and K. Wellband, H. Cayuela,
741 F. Hartmann for their constructive comments. TL and QR thank Benoit Nabholz for discussions regarding the
742 deleterious mutation loads and Hill-Robertson effects. Computations were performed on Colosse (Calcul
743 Quebec), Graham and Cedar (Compute Canada) servers. This research was carried out in conjunction with
744 EPIC4 (Enhanced Production in Coho: Culture, Community, Catch), a project supported by the government
745 of Canada through Genome Canada, Genome British Columbia, and Genome Quebec. The authors declare
746 no conflicts of interest.

747

748 **Figure Legend**

749 **Figure 1) Sampling design**

750 A) Sampling locations of 58 Coho salmon populations distributed across the species' North American range
751 of distribution. Each dot represents a sampling location. Inset: Map showing the extend of ice-sheet during
752 the Last Glacial Maximum 13 KyA. Data modified from [115]

753

754 **Figure 2) Genetic diversity and differentiation**

755 A) Linear relationship between expected heterozygosity and distance from the southernmost population
756 located in California. B) Linear increase in genetic differentiation as measured by β_{ST} as a function of the
757 distance from the southernmost population located in California. Negative values indicate the most likely
758 ancestral population. The relationship in A and B was tested using linear models. The grey vertical bar in
759 panel B) indicates the approximate location of the southern limit of the ice-sheet at the end of the last glacial
760 maxima.

761

762 **Figure 3) Genetic structure and gene flow**

763 A) Principal Component Analysis (PCA) summarising population genetic structure among 1,957 individuals
764 based on the principal component axes 1 and axes 2. Each point represents an individual and the colours
765 represent the major regional groups. B) Inference of population splits and mixture by Treemix with 4
766 statistically significant migration events ($p < 0.0001$). Bootstrap supports and migration weights are
767 indicated according to the colour scale.

768

769 **Figure 4) Inferences of demographic history using $\partial a\partial i$ and smc++**

770 A) Estimates of divergence time (in years) between each major region as inferred by $\partial a\partial i$ under the best
771 model (displayed in blue) based on the GBS SNP data set. B) Estimates of effective population size N_e for
772 each major region as inferred by $\partial a\partial i$ under each best demographic model based on the GBS SNP data set.
773 C) Estimates of migration rate among populations in neutral regions (m) of the genome and in areas of
774 restricted recombination (me) based on the GBS SNP data set. D) Estimates of effective population size (N_e)
775 change through time (in years) for the whole genome data using SMC++.

776

777 **Figure 5) Genome-wide landscapes in Coho salmon** with: A) landscape of differentiation, B) landscape of
778 genetic diversity C) divergence, D) recombination and E) gene density. Plots are averaged over 500-kb
779 windows. Only the first 16 chromosomes are displayed for simplicity. The same figure with all chromosomes
780 is available in Fig. S15.

781 **Figure 6) Linked selection revealed by correlation among different metrics**

782 Correlations between recombination rate ($\rho = 4Ne.r$) genetic diversity (π), divergence (D_{xy}) and
783 differentiation (F_{ST}) statistics (A-C), and correlation between gene density and π , D_{xy} , F_{ST} statistics (D-F).
784 Correlations between π , D_{xy} and F_{ST} statistics (G-I). The Spearman correlation values are plotted but mixed
785 linear models were fitted to further test interaction among explanatory variables (recombination rate and
786 gene density).

787
788 **Figure 7) Correlation between π_N/π_S and GC3 content for each population separately**

789 π_N/π_S is used here as a proxy for the efficacy of purifying selection with smaller values reflecting more
790 efficient purifying selection. All correlations are significant ($p < 0.001$).

791
792 **Figure 8) Analysis of deleterious load in the Coho salmon genome**

793 A) Derived allele frequency spectra across major groups. The non-synonymous variants and putatively
794 deleterious variants frequency are shown. Data are normalized for a sample of size $n = 102$ corresponding to
795 the smallest size for the combined samples in Haida Gwaii. B) Distribution of the count of homozygous
796 derived deleterious alleles in each major group. C) Distribution of the count of total derived deleterious
797 alleles in each major group. D) Correlation ($p = 0.0034$, $R^2=0.13$) between geographic distance to the
798 putative ancestral source and the distribution of homozygous derived putatively deleterious mutations.

799
800 **References:**

1. Allendorf FW. Evolution in a Toxic World. *BioScience*. 2017;67: 576–577. doi:10.1093/biosci/bix029
2. Ceballos G, Ehrlich PR, Dirzo R. Biological annihilation via the ongoing sixth mass extinction signaled by vertebrate population losses and declines. *Proc Natl Acad Sci*. 2017;114: E6089–E6096. doi:10.1073/pnas.1704949114
3. Provan J, Bennett KD. Phylogeographic insights into cryptic glacial refugia. *Trends Ecol Evol*. 2008;23: 564–571. doi:10.1016/j.tree.2008.06.010
4. Hewitt GM. Post-glacial re-colonization of European biota. *Biol J Linn Soc*. 1999;68: 87–112. doi:10.1006/bijl.1999.0332
5. Bernatchez L, Wilson CC. Comparative phylogeography of Nearctic and Palearctic fishes. *Mol Ecol*. 1998;7: 431–452. doi:10.1046/j.1365-294x.1998.00319.x
6. Frankham R, Ballou JD, Briscoe DA. Introduction to Conservation Genetics by Richard Frankham. In: Cambridge Core [Internet]. Jan 2010 [cited 2 Jul 2019]. doi:10.1017/CBO9780511809002

7. Funk WC, McKay JK, Hohenlohe PA, Allendorf FW. Harnessing genomics for delineating conservation units. *Trends Ecol Evol.* 2012;27: 489–496. doi:10.1016/j.tree.2012.05.012
8. Noor M a. F, Bennett SM. Islands of speciation or mirages in the desert? Examining the role of restricted recombination in maintaining species. *Heredity.* 2009;103: 439–444. doi:10.1038/hdy.2009.151
9. Cruickshank TE, Hahn MW. Reanalysis suggests that genomic islands of speciation are due to reduced diversity, not reduced gene flow. *Mol Ecol.* 2014;23: 3133–3157. doi:10.1111/mec.12796
10. Simons YB, Turchin MC, Pritchard JK, Sella G. The deleterious mutation load is insensitive to recent population history. *Nat Genet.* 2014;46: 220–224. doi:10.1038/ng.2896
11. Bierne N, Gagnaire P-A, David P. The geography of introgression in a patchy environment and the thorn in the side of ecological speciation. *Curr Zool.* 2013;59: 72–86. doi:10.1093/czoolo/59.1.72
12. Barton N, Bengtsson BO. The barrier to genetic exchange between hybridising populations. *Heredity.* 1986;57: 357. doi:10.1038/hdy.1986.135
13. Smith JM, Haigh J. The hitch-hiking effect of a favourable gene. *Genet Res.* 1974;23: 23–35.
14. Charlesworth B, Morgan MT, Charlesworth D. The effect of deleterious mutations on neutral molecular variation. *Genetics.* 1993;134: 1289–1303.
15. Kaplan NL, Hudson RR, Langley CH. The “hitchhiking effect” revisited. *Genetics.* 1989;123: 887–899.
16. Nordborg M, Charlesworth B, Charlesworth D. The effect of recombination on background selection. *Genet Res.* 1996;67: 159–174.
17. Payseur BA, Nachman MW. Natural selection at linked sites in humans. *Gene.* 2002;300: 31–42.
18. Hudson RR, Kaplan NL. Deleterious Background Selection with Recombination. *Genetics.* 1995;141: 1605–1617.
19. Roux C, Fraïsse C, Romiguier J, Anciaux Y, Galtier N, Bierne N. Shedding Light on the Grey Zone of Speciation along a Continuum of Genomic Divergence. *PLOS Biol.* 2016;14: e2000234. doi:10.1371/journal.pbio.2000234
20. Pouyet F, Aeschbacher S, Thiéry A, Excoffier L. Background selection and biased gene conversion affect more than 95% of the human genome and bias demographic inferences. Veeramah K, Wittkopp PJ, Gronau I, editors. *eLife.* 2018;7: e36317. doi:10.7554/eLife.36317
21. Comeron JM. Background selection as null hypothesis in population genomics: insights and challenges from *Drosophila* studies. *Philos Trans R Soc Lond B Biol Sci.* 2017;372. doi:10.1098/rstb.2016.0471
22. Simons YB, Sella G. The impact of recent population history on the deleterious mutation load in humans and close evolutionary relatives. *Curr Opin Genet Dev.* 2016;41: 150–158. doi:10.1016/j.gde.2016.09.006

23. Charlesworth D, Willis JH. The genetics of inbreeding depression. *Nat Rev Genet.* 2009;10: 783–796. doi:10.1038/nrg2664
24. Kirkpatrick M, Jarne P. The Effects of a Bottleneck on Inbreeding Depression and the Genetic Load. *Am Nat.* 2000;155: 154–167. doi:10.1086/303312
25. Charlesworth B. The Effects of Deleterious Mutations on Evolution at Linked Sites. *Genetics.* 2012;190: 5–22. doi:10.1534/genetics.111.134288
26. Robinson JA, Rääkkönen J, Vucetich LM, Vucetich JA, Peterson RO, Lohmueller KE, et al. Genomic signatures of extensive inbreeding in Isle Royale wolves, a population on the threshold of extinction. *Sci Adv.* 2019;5: eaau0757. doi:10.1126/sciadv.aau0757
27. Robinson JA, Ortega-Del Vecchyo D, Fan Z, Kim BY, vonHoldt BM, Marsden CD, et al. Genomic Flatlining in the Endangered Island Fox. *Curr Biol CB.* 2016;26: 1183–1189. doi:10.1016/j.cub.2016.02.062
28. Abascal F, Corvelo A, Cruz F, Villanueva-Cañas JL, Vlasova A, Marcet-Houben M, et al. Extreme genomic erosion after recurrent demographic bottlenecks in the highly endangered Iberian lynx. *Genome Biol.* 2016;17: 251. doi:10.1186/s13059-016-1090-1
29. Dobrynin P, Liu S, Tamazian G, Xiong Z, Yurchenko AA, Krasheninnikova K, et al. Genomic legacy of the African cheetah, *Acinonyx jubatus*. *Genome Biol.* 2015;16: 277. doi:10.1186/s13059-015-0837-4
30. Yang Y, Ma T, Wang Z, Lu Z, Li Y, Fu C, et al. Genomic effects of population collapse in a critically endangered ironwood tree *Ostrya rehderiana*. *Nat Commun.* 2018;9: 5449. doi:10.1038/s41467-018-07913-4
31. Xue Y, Prado-Martinez J, Sudmant PH, Narasimhan V, Ayub Q, Szpak M, et al. Mountain gorilla genomes reveal the impact of long-term population decline and inbreeding. *Science.* 2015;348: 242–245. doi:10.1126/science.aaa3952
32. Grossen C, Guillaume F, Keller LF, Croll D. Accumulation and purging of deleterious mutations through severe bottlenecks in ibex. *bioRxiv.* 2019; 605147. doi:10.1101/605147
33. Henn BM, Botigué LR, Peischl S, Dupanloup I, Lipatov M, Maples BK, et al. Distance from sub-Saharan Africa predicts mutational load in diverse human genomes. *Proc Natl Acad Sci.* 2016;113: E440–E449. doi:10.1073/pnas.1510805112
34. Henn BM, Botigué LR, Bustamante CD, Clark AG, Gravel S. Estimating the mutation load in human genomes. *Nat Rev Genet.* 2015;16: 333–343. doi:10.1038/nrg3931
35. Krkosek M, Ford JS, Morton A, Lele S, Myers RA, Lewis MA. Declining wild salmon populations in relation to parasites from farm salmon. *Science.* 2007;318: 1772–1775. doi:10.1126/science.1148744
36. Irvine JR, Fukuwaka M. Pacific salmon abundance trends and climate change. *ICES J Mar Sci.* 2011;68: 1122–1130. doi:10.1093/icesjms/fsq199
37. Gustafson RG, Waples RS, Myers JM, Weitkamp LA, Bryant GJ, Johnson OW, et al. Pacific Salmon Extinctions: Quantifying Lost and Remaining Diversity. *Conserv Biol.* 2007;21: 1009–1020. doi:10.1111/j.1523-1739.2007.00693.x

38. Smith CT, Nelson RJ, Wood CC, Koop BF. Glacial biogeography of North American coho salmon (*Oncorhynchus kisutch*). *Mol Ecol*. 2001;10: 2775–2785.
39. Beacham TD, Wetklo M, Deng L, MacConnachie C. Coho Salmon Population Structure in North America Determined from Microsatellites. *Trans Am Fish Soc*. 2011;140: 253–270. doi:10.1080/00028487.2011.558782
40. McPhail JD, Lindsey CC. Freshwater fishes of northwestern Canada and Alaska. Fisheries Research Board of Canada : available by mail from the Queen’s Printer; 1970.
41. UBC Press | Pacific Salmon Life Histories, By Cornelis Groot, Leo Margolis and Leo Margolis. In: UBC Press [Internet]. [cited 1 Jul 2019]. Available: <https://www.ubcpres.ca/pacific-salmon-life-histories>
42. Hocutt CH, Wiley EO, editors. The Zoogeography of North American Freshwater Fishes. 1 edition. New York: Wiley-Interscience; 1986.
43. Mee JA, Moore J-S. The ecological and evolutionary implications of microrefugia. *J Biogeogr*. 2014;41: 837–841. doi:10.1111/jbi.12254
44. Warner BG, Mathewes RW, Clague JJ. Ice-free conditions on the queen charlotte islands, british columbia, at the height of late wisconsin glaciation. *Science*. 1982;218: 675–677. doi:10.1126/science.218.4573.675
45. Cubry P, Vigouroux Y, François O. The Empirical Distribution of Singletons for Geographic Samples of DNA Sequences. *Front Genet*. 2017;8. doi:10.3389/fgene.2017.00139
46. Weir BS, Goudet J. A Unified Characterization of Population Structure and Relatedness. *Genetics*. 2017;206: 2085–2103. doi:10.1534/genetics.116.198424
47. Weir BS, Cockerham CC. Estimating F-Statistics for the Analysis of Population Structure. *Evolution*. 1984;38: 1358–1370. doi:10.2307/2408641
48. Ward RD, Woodwark M, Skibinski DOF. A comparison of genetic diversity levels in marine, freshwater, and anadromous fishes. *J Fish Biol*. 1994;44: 213–232. doi:10.1111/j.1095-8649.1994.tb01200.x
49. Pickrell JK, Pritchard JK. Inference of Population Splits and Mixtures from Genome-Wide Allele Frequency Data. *PLOS Genet*. 2012;8: e1002967. doi:10.1371/journal.pgen.1002967
50. Gutenkunst RN, Hernandez RD, Williamson SH, Bustamante CD. Inferring the Joint Demographic History of Multiple Populations from Multidimensional SNP Frequency Data. *PLOS Genet*. 2009;5: e1000695. doi:10.1371/journal.pgen.1000695
51. Roux C, Tsagkogeorga G, Bierne N, Galtier N. Crossing the species barrier: genomic hotspots of introgression between two highly divergent *Ciona intestinalis* species. *Mol Biol Evol*. 2013;30: 1574–1587. doi:10.1093/molbev/mst066
52. COSEWIC assessment and status report on the coho salmon *Oncorhynchus kisutch* (Interior Fraser population) in Canada - Species at Risk Public Registry [Internet]. [cited 1 Jul 2019]. Available: https://wildlife-species.canada.ca/species-risk-registry/document/default_e.cfm?documentID=105

53. Terhorst J, Kamm JA, Song YS. Robust and scalable inference of population history from hundreds of unphased whole genomes. *Nat Genet.* 2017;49: 303–309. doi:10.1038/ng.3748
54. Haenel Q, Laurentino TG, Roesti M, Berner D. Meta-analysis of chromosome-scale crossover rate variation in eukaryotes and its significance to evolutionary genomics. *Mol Ecol.* 2018;27: 2477–2497. doi:10.1111/mec.14699
55. Eyre-Walker Adam. Recombination and mammalian genome evolution. *Proc R Soc Lond B Biol Sci.* 1993;252: 237–243. doi:10.1098/rspb.1993.0071
56. Galtier N, Piganeau G, Mouchiroud D, Duret L. GC-Content Evolution in Mammalian Genomes: The Biased Gene Conversion Hypothesis. *Genetics.* 2001;159: 907–911.
57. Christensen KA, Leong JS, Sakhrani D, Biagi CA, Minkley DR, Withler RE, et al. Chinook salmon (*Oncorhynchus tshawytscha*) genome and transcriptome. *PLOS ONE.* 2018;13: e0195461. doi:10.1371/journal.pone.0195461
58. Gao L, Jia J, Kong X. A SNP-Based Molecular Barcode for Characterization of Common Wheat. *PLOS ONE.* 2016;11: e0150947. doi:10.1371/journal.pone.0150947
59. Yáñez JM, Naswa S, López ME, Bassini L, Correa K, Gilbey J, et al. Genomewide single nucleotide polymorphism discovery in Atlantic salmon (*Salmo salar*): validation in wild and farmed American and European populations. *Mol Ecol Resour.* 2016;16: 1002–1011. doi:10.1111/1755-0998.12503
60. Li JZ, Absher DM, Tang H, Southwick AM, Casto AM, Ramachandran S, et al. Worldwide human relationships inferred from genome-wide patterns of variation. *Science.* 2008;319: 1100–1104. doi:10.1126/science.1153717
61. Wakeley J. *Coalescent Theory: An Introduction.* 1st edition. Greenwood Village, Colo: W. H. Freeman; 2008.
62. Alcalá Nicolas, Vuilleumier Séverine. Turnover and accumulation of genetic diversity across large time-scale cycles of isolation and connection of populations. *Proc R Soc B Biol Sci.* 2014;281: 20141369. doi:10.1098/rspb.2014.1369
63. Shafer ABA, Cullingham CI, Côté SD, Coltman DW. Of glaciers and refugia: a decade of study sheds new light on the phylogeography of northwestern North America. *Mol Ecol.* 2010;19: 4589–4621. doi:10.1111/j.1365-294X.2010.04828.x
64. O'Reilly P, Reimchen TE, Beech R, Strobeck C. MITOCHONDRIAL DNA IN GASTEROSTEUS AND PLEISTOCENE GLACIAL REFUGIUM ON THE QUEEN CHARLOTTE ISLANDS, BRITISH COLUMBIA. *Evol Int J Org Evol.* 1993;47: 678–684. doi:10.1111/j.1558-5646.1993.tb02122.x
65. Pruett CL, Topp CM, Maley JM, McCracken K, Rohwer S, Birks S, et al. Evidence from the genetics of landbirds for a forested pleistocene glacial refugium in the haida gwaii area. *Condor.* 2013;115: 725–737. doi:10.1525/cond.2013.120123
66. Geraldés A, Askelson KK, Nikelski E, Doyle FI, Harrower WL, Winker K, et al. Population genomic analyses reveal a highly differentiated and endangered genetic cluster of northern goshawks (*Accipiter gentilis laingi*) in Haida Gwaii. *Evol Appl.* 2019;12: 757–772. doi:10.1111/eva.12754

67. Gómez A, Lunt DH. Refugia within Refugia: Patterns of Phylogeographic Concordance in the Iberian Peninsula. In: Weiss S, Ferrand N, editors. *Phylogeography of Southern European Refugia: Evolutionary perspectives on the origins and conservation of European biodiversity*. Dordrecht: Springer Netherlands; 2007. pp. 155–188. doi:10.1007/1-4020-4904-8_5
68. Brown LR, Moyle PB, Yoshiyama RM. Historical Decline and Current Status of Coho Salmon in California. *North Am J Fish Manag*. 1994;14: 237–261. doi:10.1577/1548-8675(1994)014<0237:HDACSO>2.3.CO;2
69. Petit RJ, Aguinagalde I, Beaulieu J-L de, Bittkau C, Brewer S, Cheddadi R, et al. Glacial Refugia: Hotspots But Not Melting Pots of Genetic Diversity. *Science*. 2003;300: 1563–1565. doi:10.1126/science.1083264
70. Waples RS, Teel DJ, Myers JM, Marshall AR. Life-History Divergence in Chinook Salmon: Historic Contingency and Parallel Evolution. *Evolution*. 2004;58: 386–403. doi:10.1111/j.0014-3820.2004.tb01654.x
71. Burri R. Linked selection, demography and the evolution of correlated genomic landscapes in birds and beyond. *Mol Ecol*. 2017;26: 3853–3856. doi:10.1111/mec.14167
72. Stankowski S, Chase MA, Fuiten AM, Rodrigues MF, Ralph PL, Streisfeld MA. Widespread selection and gene flow shape the genomic landscape during a radiation of monkeyflowers. *bioRxiv*. 2019; 342352. doi:10.1101/342352
73. Burri R, Nater A, Kawakami T, Mugal CF, Olason PI, Smeds L, et al. Linked selection and recombination rate variation drive the evolution of the genomic landscape of differentiation across the speciation continuum of *Ficedula* flycatchers. *Genome Res*. 2015;25: 1656–1665. doi:10.1101/gr.196485.115
74. Ravinet M, Faria R, Butlin RK, Galindo J, Bierne N, Rafajlović M, et al. Interpreting the genomic landscape of speciation: a road map for finding barriers to gene flow. *J Evol Biol*. 2017;30: 1450–1477. doi:10.1111/jeb.13047
75. Burri R. Dissecting differentiation landscapes: a linked selection’s perspective. *J Evol Biol*. 2017;30: 1501–1505. doi:10.1111/jeb.13108
76. Rougemont Q, Bernatchez L. The demographic history of Atlantic salmon (*Salmo salar*) across its distribution range reconstructed from approximate Bayesian computations*. *Evolution*. 2018;72: 1261–1277. doi:10.1111/evo.13486
77. Vijay N, Bossu CM, Poelstra JW, Weissensteiner MH, Suh A, Kryukov AP, et al. Evolution of heterogeneous genome differentiation across multiple contact zones in a crow species complex. *Nat Commun*. 2016;7: 13195. doi:10.1038/ncomms13195
78. Van Doren BM, Campagna L, Helm B, Illera JC, Lovette IJ, Liedvogel M. Correlated patterns of genetic diversity and differentiation across an avian family. *Mol Ecol*. 2017;26: 3982–3997. doi:10.1111/mec.14083
79. Macqueen DJ, Johnston IA. A well-constrained estimate for the timing of the salmonid whole genome duplication reveals major decoupling from species diversification. *Proc R Soc B Biol Sci*. 2014;281. doi:10.1098/rspb.2013.2881
80. Kodama M, Briec MSO, Devlin RH, Hard JJ, Naish KA. Comparative mapping between Coho Salmon (*Oncorhynchus kisutch*) and three other salmonids suggests a role for

- chromosomal rearrangements in the retention of duplicated regions following a whole genome duplication event. *G3 Bethesda Md.* 2014;4: 1717–1730. doi:10.1534/g3.114.012294
81. Briec MSO, Ono K, Drinan DP, Naish KA. Integration of Random Forest with population-based outlier analyses provides insight on the genomic basis and evolution of run timing in Chinook salmon (*Oncorhynchus tshawytscha*). *Mol Ecol.* 2015;24: 2729–2746. doi:10.1111/mec.13211
 82. Lien S, Koop BF, Sandve SR, Miller JR, Kent MP, Nome T, et al. The Atlantic salmon genome provides insights into rediploidization. *Nature.* 2016;533: 200–205. doi:10.1038/nature17164
 83. Sutherland BJB, Rico C, Audet C, Bernatchez L. Sex Chromosome Evolution, Heterochiasmy, and Physiological QTL in the Salmonid Brook Charr *Salvelinus fontinalis*. *G3 Bethesda Md.* 2017;7: 2749–2762. doi:10.1534/g3.117.040915
 84. Allendorf FW, Bassham S, Cresko WA, Limborg MT, Seeb LW, Seeb JE. Effects of crossovers between homeologs on inheritance and population genomics in polyploid-derived salmonid fishes. *J Hered.* 2015;106: 217–227. doi:10.1093/jhered/esv015
 85. Eyre-Walker A, Keightley PD. The distribution of fitness effects of new mutations. *Nat Rev Genet.* 2007;8: 610–618. doi:10.1038/nrg2146
 86. Marsden CD, Vecchyo DO-D, O’Brien DP, Taylor JF, Ramirez O, Vilà C, et al. Bottlenecks and selective sweeps during domestication have increased deleterious genetic variation in dogs. *Proc Natl Acad Sci.* 2016;113: 152–157. doi:10.1073/pnas.1512501113
 87. Roze D, Barton NH. The Hill-Robertson effect and the evolution of recombination. *Genetics.* 2006;173: 1793–1811. doi:10.1534/genetics.106.058586
 88. Zhou Y, Massonnet M, Sanjak JS, Cantu D, Gaut BS. Evolutionary genomics of grape (*Vitis vinifera* ssp. *vinifera*) domestication. *Proc Natl Acad Sci.* 2017;114: 11715–11720. doi:10.1073/pnas.1709257114
 89. Peischl S, Dupanloup I, Kirkpatrick M, Excoffier L. On the accumulation of deleterious mutations during range expansions. *Mol Ecol.* 2013;22: 5972–5982. doi:10.1111/mec.12524
 90. Peischl S, Dupanloup I, Foucal A, Jomphe M, Bruat V, Grenier J-C, et al. Relaxed Selection During a Recent Human Expansion. *Genetics.* 2018;208: 763–777. doi:10.1534/genetics.117.300551
 91. Laenen B, Tedder A, Nowak MD, Toräng P, Wunder J, Wötzel S, et al. Demography and mating system shape the genome-wide impact of purifying selection in *Arabis alpina*. *Proc Natl Acad Sci.* 2018;115: 816–821. doi:10.1073/pnas.1707492115
 92. Robinson JA, Brown C, Kim BY, Lohmueller KE, Wayne RK. Purging of Strongly Deleterious Mutations Explains Long-Term Persistence and Absence of Inbreeding Depression in Island Foxes. *Curr Biol CB.* 2018;28: 3487-3494.e4. doi:10.1016/j.cub.2018.08.066
 93. Kim BY, Huber CD, Lohmueller KE. Deleterious variation shapes the genomic landscape of introgression. *PLOS Genet.* 2018;14: e1007741. doi:10.1371/journal.pgen.1007741

94. Haddrill PR, Halligan DL, Tomaras D, Charlesworth B. Reduced efficacy of selection in regions of the *Drosophila* genome that lack crossing over. *Genome Biol.* 2007;8: R18. doi:10.1186/gb-2007-8-2-r18
95. Rodgers-Melnick E, Bradbury PJ, Elshire RJ, Glaubitz JC, Acharya CB, Mitchell SE, et al. Recombination in diverse maize is stable, predictable, and associated with genetic load. *Proc Natl Acad Sci.* 2015;112: 3823–3828. doi:10.1073/pnas.1413864112
96. Torres R, Stetter MG, Hernandez RD, Ross-Ibarra J. The temporal dynamics of background selection in non-equilibrium populations. *bioRxiv.* 2019; 618389. doi:10.1101/618389
97. Moore J-S, Harris LN, Le Luyer J, Sutherland BJJ, Rougemont Q, Tallman RF, et al. Genomics and telemetry suggest a role for migration harshness in determining overwintering habitat choice, but not gene flow, in anadromous Arctic Char. *Mol Ecol.* 2017;26: 6784–6800. doi:10.1111/mec.14393
98. Catchen JM, Hohenlohe PA, Bernatchez L, Funk WC, Andrews KR, Allendorf FW. Unbroken: RADseq remains a powerful tool for understanding the genetics of adaptation in natural populations. *Mol Ecol Resour.* 2017;17: 362–365. doi:10.1111/1755-0998.12669
99. Danecek P, Auton A, Abecasis G, Albers CA, Banks E, DePristo MA, et al. The variant call format and VCFtools. *Bioinforma Oxf Engl.* 2011;27: 2156–2158. doi:10.1093/bioinformatics/btr330
100. Goudet J. hierfstat, a package for r to compute and test hierarchical F-statistics. *Mol Ecol Notes.* 2005;5: 184–186. doi:10.1111/j.1471-8286.2004.00828.x
101. Frichot E, François O. LEA: An R package for landscape and ecological association studies. *Methods Ecol Evol.* 2015;6: 925–929. doi:10.1111/2041-210X.12382
102. Alexander DH, Novembre J, Lange K. Fast model-based estimation of ancestry in unrelated individuals. *Genome Res.* 2009;19: 1655–1664. doi:10.1101/gr.094052.109
103. Dray S, Dufour A-B. The ade4 Package: Implementing the Duality Diagram for Ecologists. *J Stat Softw.* 2007;22: 1–20.
104. Rougemont Q, Gagnaire P-A, Perrier C, Genthon C, Besnard A-L, Launey S, et al. Inferring the demographic history underlying parallel genomic divergence among pairs of parasitic and nonparasitic lamprey ecotypes. *Mol Ecol.* 2017;26: 142–162. doi:10.1111/mec.13664
105. Chen S, Zhou Y, Chen Y, Gu J. fastp: an ultra-fast all-in-one FASTQ preprocessor. *Bioinforma Oxf Engl.* 2018;34: i884–i890. doi:10.1093/bioinformatics/bty560
106. Li H. Aligning sequence reads, clone sequences and assembly contigs with BWA-MEM. *ArXiv13033997 Q-Bio.* 2013; Available: <http://arxiv.org/abs/1303.3997>
107. DePristo MA, Banks E, Poplin R, Garimella KV, Maguire JR, Hartl C, et al. A framework for variation discovery and genotyping using next-generation DNA sequencing data. *Nat Genet.* 2011;43: 491. doi:10.1038/ng.806
108. Wickham H. ggplot2: Elegant Graphics for Data Analysis [Internet]. New York: Springer-Verlag; 2009. Available: <https://www.springer.com/gp/book/9780387981413>

109. McVean G, Awadalla P, Fearnhead P. A Coalescent-Based Method for Detecting and Estimating Recombination From Gene Sequences. *Genetics*. 2002;160: 1231–1241.
110. Martin S. https://github.com/simonhmartin/genomics_general.
https://github.com/simonhmartin/genomics_general.
111. Leroy T, Anselmetti Y, Tilak M-K, Bérard S, Csukonyi L, Gabrielli M, et al. A bird's white-eye view on neosex chromosome evolution. *bioRxiv*. 2019; 505610. doi:10.1101/505610
112. Choi Y, Sims GE, Murphy S, Miller JR, Chan AP. Predicting the functional effect of amino acid substitutions and indels. *PloS One*. 2012;7: e46688. doi:10.1371/journal.pone.0046688
113. Bates D, Mächler M, Bolker B, Walker S. Fitting Linear Mixed-Effects Models Using lme4. *J Stat Softw*. 2015;67: 1–48. doi:10.18637/jss.v067.i01
114. Cingolani P, Platts A, Wang LL, Coon M, Nguyen T, Wang L, et al. A program for annotating and predicting the effects of single nucleotide polymorphisms, SnpEff: SNPs in the genome of *Drosophila melanogaster* strain w1118; iso-2; iso-3. *Fly (Austin)*. 2012;6: 80–92. doi:10.4161/fly.19695
115. Government of Canada NRC. GEOSCAN Search Results: Fastlink [Internet]. 7 Dec 2015 [cited 26 Jul 2019]. Available: <https://geoscan.nrcan.gc.ca/starweb/geoscan/servlet.starweb?path=geoscan/fulle.web&search1=R=214399>

801 **Supporting Information Legend**

802

803 **S1 Fig. Linear decrease in genetic diversity when considering π SNP as a function of the distance to the**
804 **southernmost sample site.** Each points represents a sample site and is coloured by region.

805

806 **S2 Fig. Network of shared and private polymorphisms.** The branch (grey) represent shared polymorphism
807 between sample site and are proportional to levels of sharing. Each point represent the number of private
808 polymorphisms and is coloured by region. Computation were based on a sample of size 100 in each region to
809 enable comparison.

810

811 **S3 Fig. Measure of linkage disequilibrium decay using whole genome sequencing data.** LD between
812 pairs of loci was measured as r^2 in windows of 1 million base pairs. Means smoothed value are display for
813 each whole genome samples.

814

815 **S4 Fig. Patterns of Isolation By Distance.** Increasing F_{ST} as a function of the distance to the southernmost
816 site. Each points represents a sample site and is coloured by region.

817

818 **S5 Fig. Summaries of F_{ST} values.**

819 A. F_{ST} -based Hierarchical tree depicting relationship among samples. Colors represent the major region.

820 B. Heatmap of F_{ST} values among samples ordered from North to South on the X and Y-axis.

821

822 **S6 Fig. Structure and Admixture inferences.**

823 A. Admixture Barplot obtained from LEA for various K-values.

824 B. Progressive decrease of LEA cross-entropy criterion. Lower cross-entropy values indicates the number of
825 cluster compatible with the data (here from 30 to 60).

826

827 **S7 Fig. Multidimensional Scaling (MDS) plot depicting relationship among individuals.** Each points
828 represents an individual site and is coloured by region.

829

830 **S8 Fig. Principal Component Analysis recapitulating the relationship among individuals.** The Axis 3
831 and axis 4 are displayed.

832

833 **S9 Fig. Treemix results**

834 A. Proportion of variance explained (y-axis) as a function of the number of migration edge (x-axis)

835 B. Treemix tree inferred without gene flow and residuals

836 C. Residuals for Treemix tree with four migration edges

837

838 **S10 Fig. Compared Demographic Models**

839 Strict Isolation (SI), Isolation with constant Migration (IM), Ancient Migration (AM) and Secondary
840 Contact (SC). The models shared the following parameters: Tsplit: number of generation of divergence
841 (backwards in time). N_{anc} , N_1 , N_2 : effective population size of the ancestral population, of the first and
842 second daughter population. M_1 and M_2 represent the effective migration rates per generation with m the
843 proportion of population made of migrants from the other population. Tsc is the number of generations since
844 gene flow started (secondary contact) after a period of isolation. Tam is the number of generations since the
845 two populations have diverged without gene flow. Each models are declined in alternative version allowing
846 homogeneous or heterogeneous gene flow and homogeneous and heterogeneous effective size to account for
847 the effect of linked selection (affecting N_e) and barrier to gene flow (affecting m).

848

849 **S11 Fig. Estimate of effective population size across models with linked selection (2N suffix) and
850 barriers to gene flow (2m suffix).** AM2m = Ancient Migration with heterogeneous migration.

851 AM2N = Ancient Migration with heterogeneous effective population size. IM2m = Isolation with Migration
852 with heterogeneous migration. IM2N2m = Isolation with Migration with heterogeneous migration and with
853 heterogeneous effective population size, SC2m = Secondary Contact with heterogeneous migration.
854 SC2N2m = Secondary Contact with heterogeneous migration and with heterogeneous effective population
855 size.

856

857 **S12 Fig. SMC++ estimates of effective population sizes for the 11 whole genome samples included.**

858

859 **S13 Fig. SMC++ estimates of divergence time between all possible pairs of joint Site Frequency
860 Spectra based on WGS data.** Two estimates of mutation rate were used. One standard estimate of $1.25e-8$
861 μ /bp/generation and a second based on unpublished data.

862

863 **S14 Fig. Negative Relationship between effective recombination rate (ρ) and length of chromosome
864 in bp.**

865

866 **S15 Fig. Genome-wide landscapes in coho salmon with (A) landscape of differentiation, B) landscape
867 of genetic diversity C) divergence, D) recombination E) gene density, plots are averaged over 500kb
868 windows.** The figure is the same as figure 5 but all the 30 chromosomes are displayed.

869

870 **S16 Fig. Correlation between π_N/π_S and effective population size (N_e) during postglacial time.** Each
871 point represent a sample locality and is color coded by region.

872

873 **S17 Fig. DAF spectrum of nonsynonymous and putatively deleterious mutation in each region for all
874 samples.**

875

876 **S18 Fig. Significant mean derived allele frequencies of deleterious mutation.** Displayed are the mean
877 derived allele frequencies of polymorphic deleterious sites in each regions +/- 2 standard deviation.
878 x-axis = chromosome position (in bp) and y-axis = effective recombination landscape. Each red dots
879 represents a candidate deleterious mutation.

880

881 **S19 Fig. Location of putatively deleterious mutation along the effective recombination landscape.**

882

883 **S20 Fig : Positive correlation between chromosome length and occurrence of deleterious variants along
884 chromosome.**

885

886 **Table Legend:**

887

888 **S1 Table:** Abbreviation, Region and coordinates (Longitude and Latitude) of each river used in the GBS data
889 with the number of individuals provided (nb. Inds).

890

891 **S2 Table:** River Name, region and coordinates (Longitude and Latitude) of each river used in the whole
892 genome resequencing data.

893

894 **S3 Table:** BST values along with 95% confidence intervals for each river from the GBS data (82 K SNPs).
895 95% confidence intervals obtained after 1000 bootstraps.

896

897 **S4 Table:** Distribution of singleton in the WGS data. The Thompson sample displays less singleton than
898 southern samples.

899

900 **S5 Table:** model choice results for dadi. AIC and deltaAIC are provided for each pairwise comparison and
901 model. AM = Ancient Migration, IM = Isolation with Migration, SI = Strict Isolation, SC = Secondary
902 Contact, the simplest models assume homogeneous migration and homogeneous effective population size.
903 2N suffix = heterogeneous effective population size, 2Msuffix = heterogeneous migration.

904 Model with both suffix assumes that both effective population size and migration are heterogeneous.

905 Modil with a single suffix assumes that either migration or effective population size are heterogeneous.

906

907 **S6 Table :** Parameter estimates from GBS data obtained under the best demographic model with dadi.

908 Ne1 and Ne2, effective population size of the compared pair. $m1 \leftarrow 2$ and $m2 \leftarrow 1$, migration from
909 population 2 to population 1 and migration from population 1 into population 2. me12 and me21, effective
910 migration rate estimated in the most differentiated regions of the genome Ts: Split Time of the ancestral
911 population in two population; Tsc: duration of the secondary contact P: proportion of the genome freely
912 exchanged (1-P provides the proportion of the genome non-neutrally exchanged); Q: proportion of the
913 genome with a reduced effective population size due to selection at linked sites; hrf = Hill-Robertson factor
914 representing the reduction of Ne in the region Q with reduced Ne.

915

916 **S7 Table:** PCA loadings for Dxy, Fst and Pi.

917

918 **S8 Table:** A) Spearman correlation association to the comparison in Figure 6.

919 B) Linear models testing the combined effect of recombination (Rho) and gene density (Gene count).

920 Interaction terms were not significant for Pi and Dxy and were removed.

921 **S9 Table:** spearman correlation obtained between recombination and Dxy, Fst and Pi when considering each
922 possible pairs of river separately (n = 55) or each river independently (for Pi only).

923

924 **S10 Table:** Results of linear models testing the correlation between piN/piS and GC3.

925

926 **S11 Table:** Summary of deleterious variation by region.

927 1) Derived Allele Frequency (DAF) of deleterious mutation, after averaging by rivers and then by major

928 regional group. 2) Count of deleterious mutations in each rivers and then averaged by major regional group.

929 3) Number of homozygous derived deleterious mutations by individual, after averaging by rivers and then

930 by major regional group. 4) Number of heterozygous mutations by individuals, after averaging by rivers and

931 then by major regional group 5) Total load of derived deleterious mutations by individuals, after averaging

932 by rivers and then by major regional group.

933

934 **S12 Table:** Results of Wilcoxon test (Man-Whitney tests) for differences in derived allele frequencies
935 among major groups for a sample of size 100.

936

937 **S13 Table:** Results of Wilcoxon test (Man-Whitney tests) for differences in count of derived homozygous
938 variants and total load among individuals in each region.

939

940 **S14 Table:** SNPEff results classified by categories for the deleterious mutations identified in the GBS data.

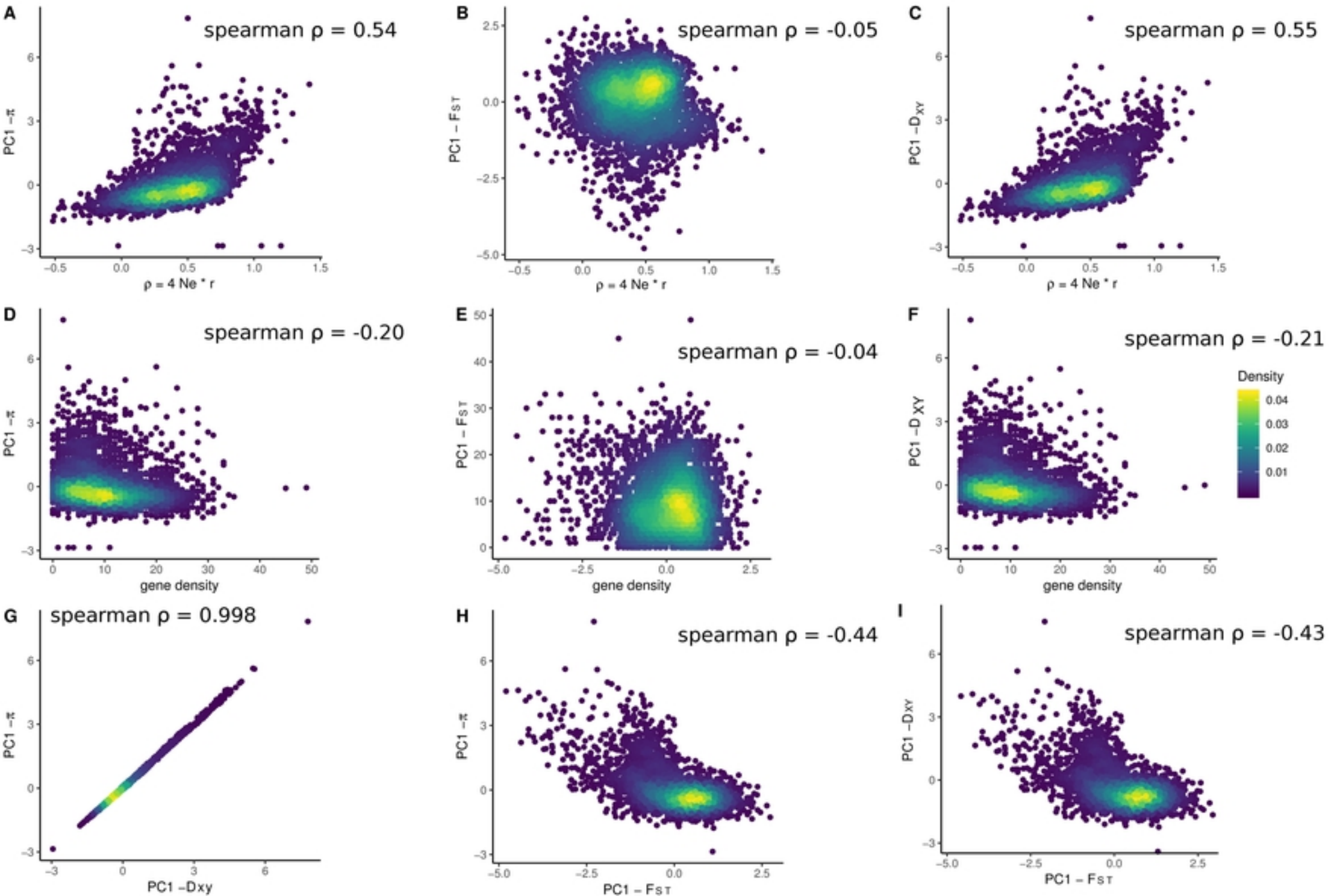


Fig 6

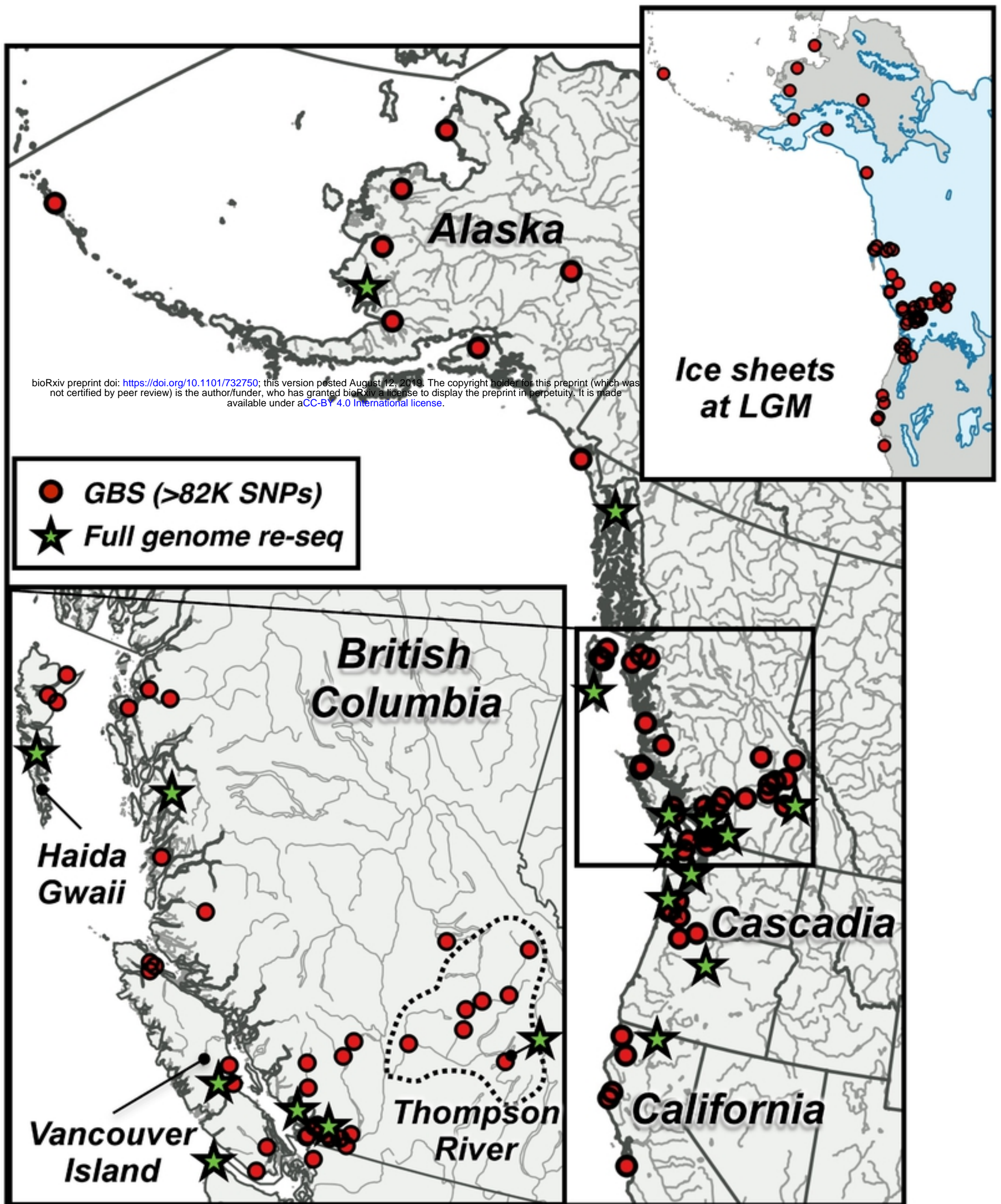


Fig 1

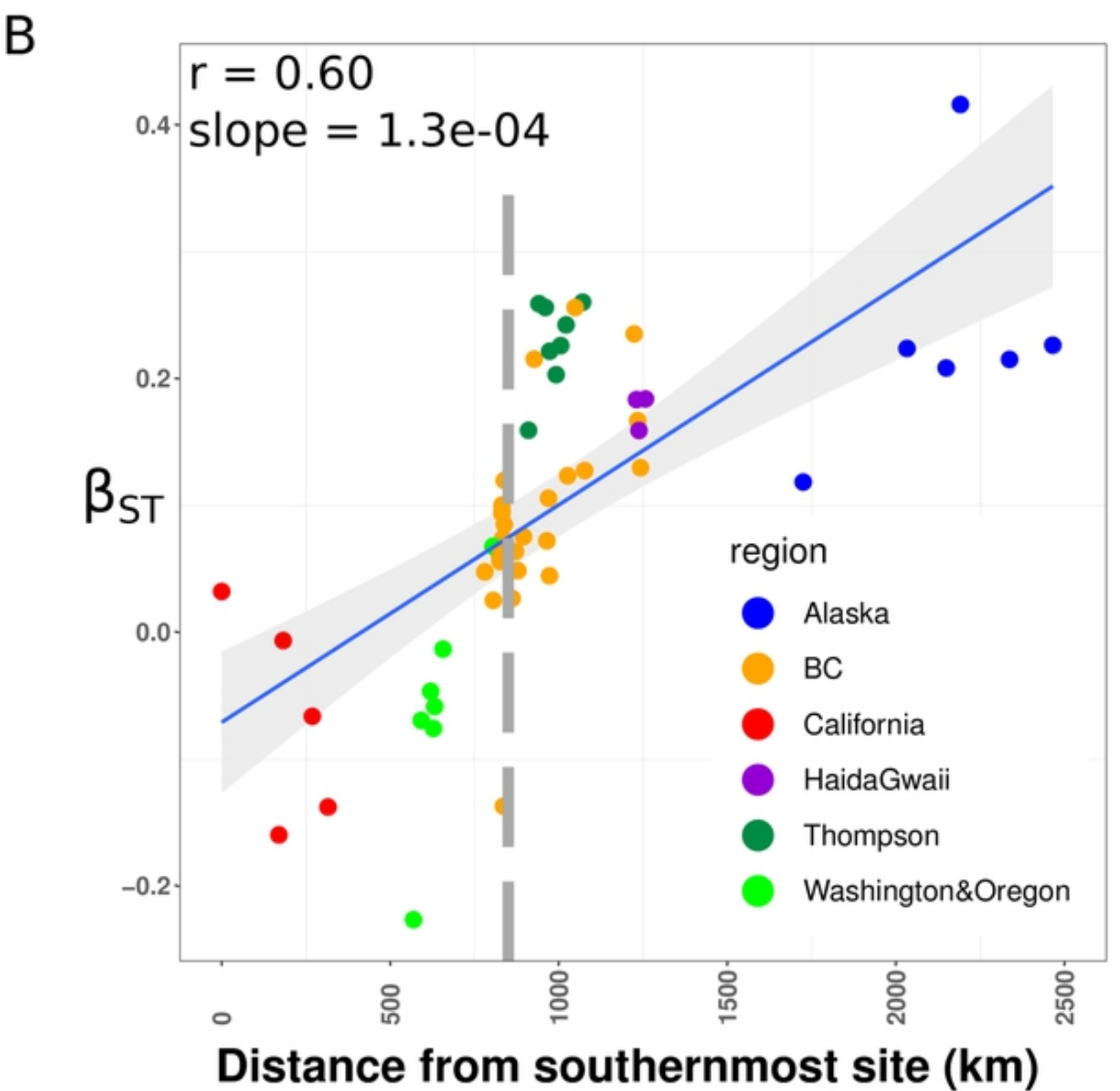
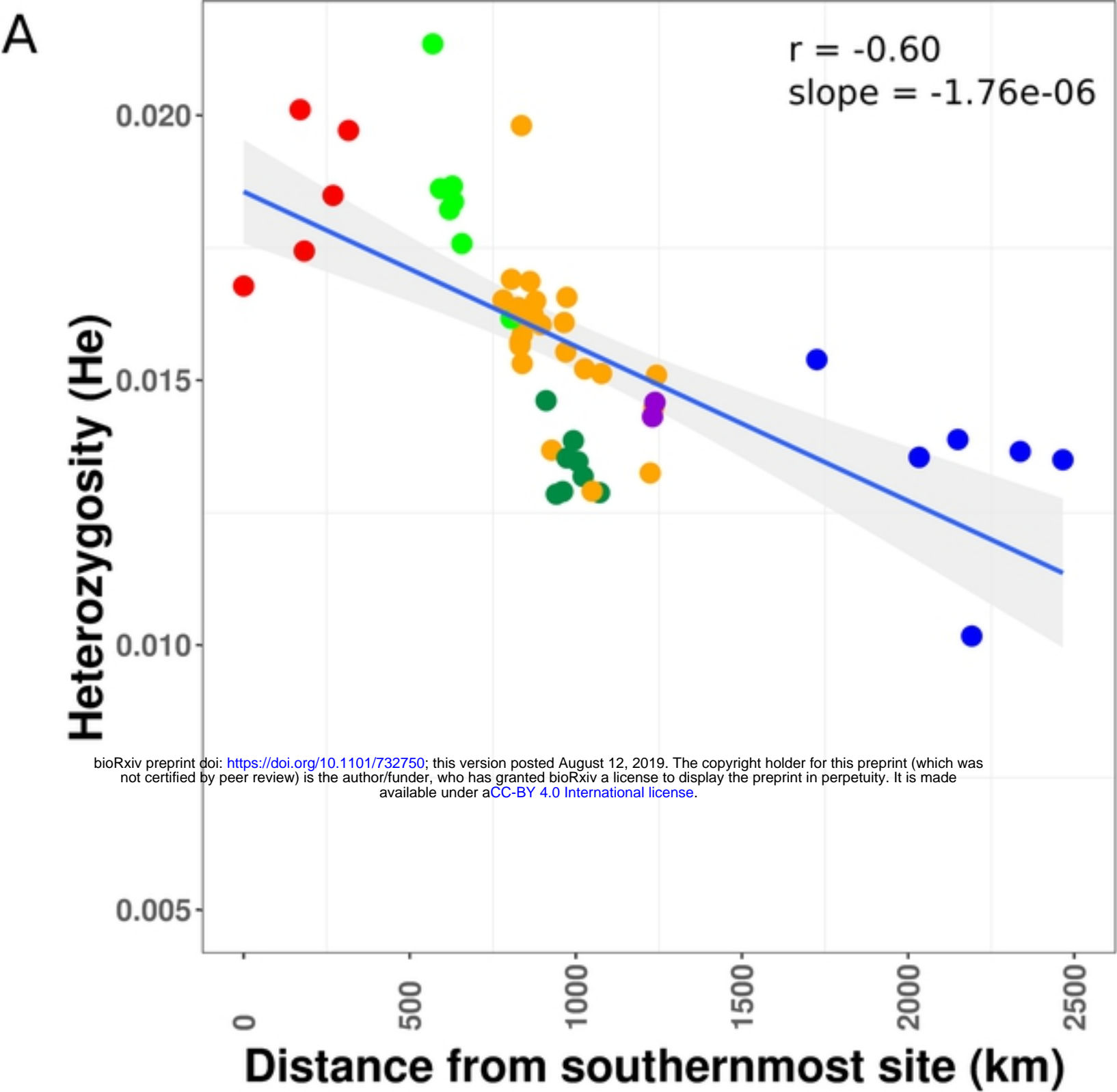


Fig 2

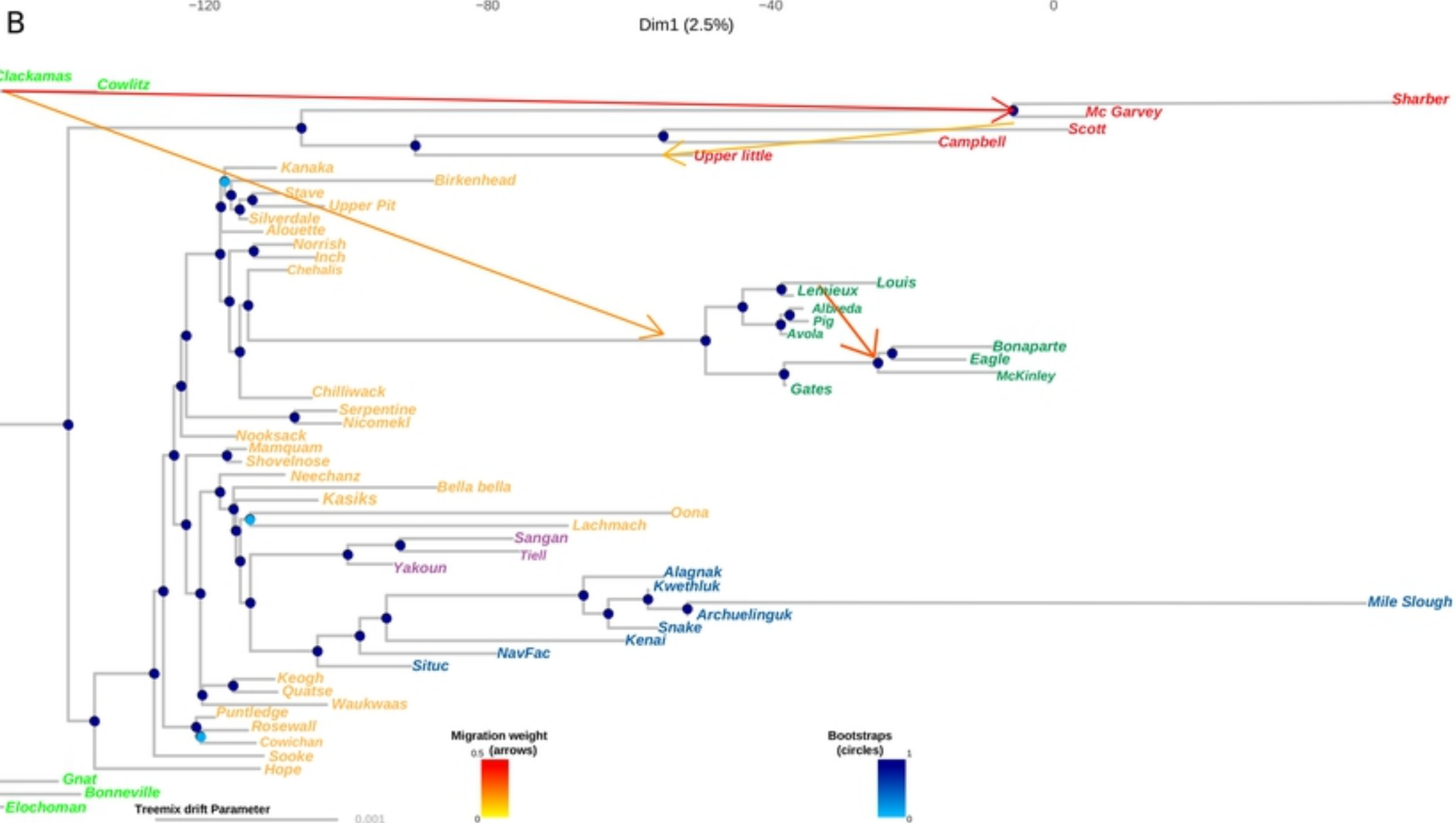
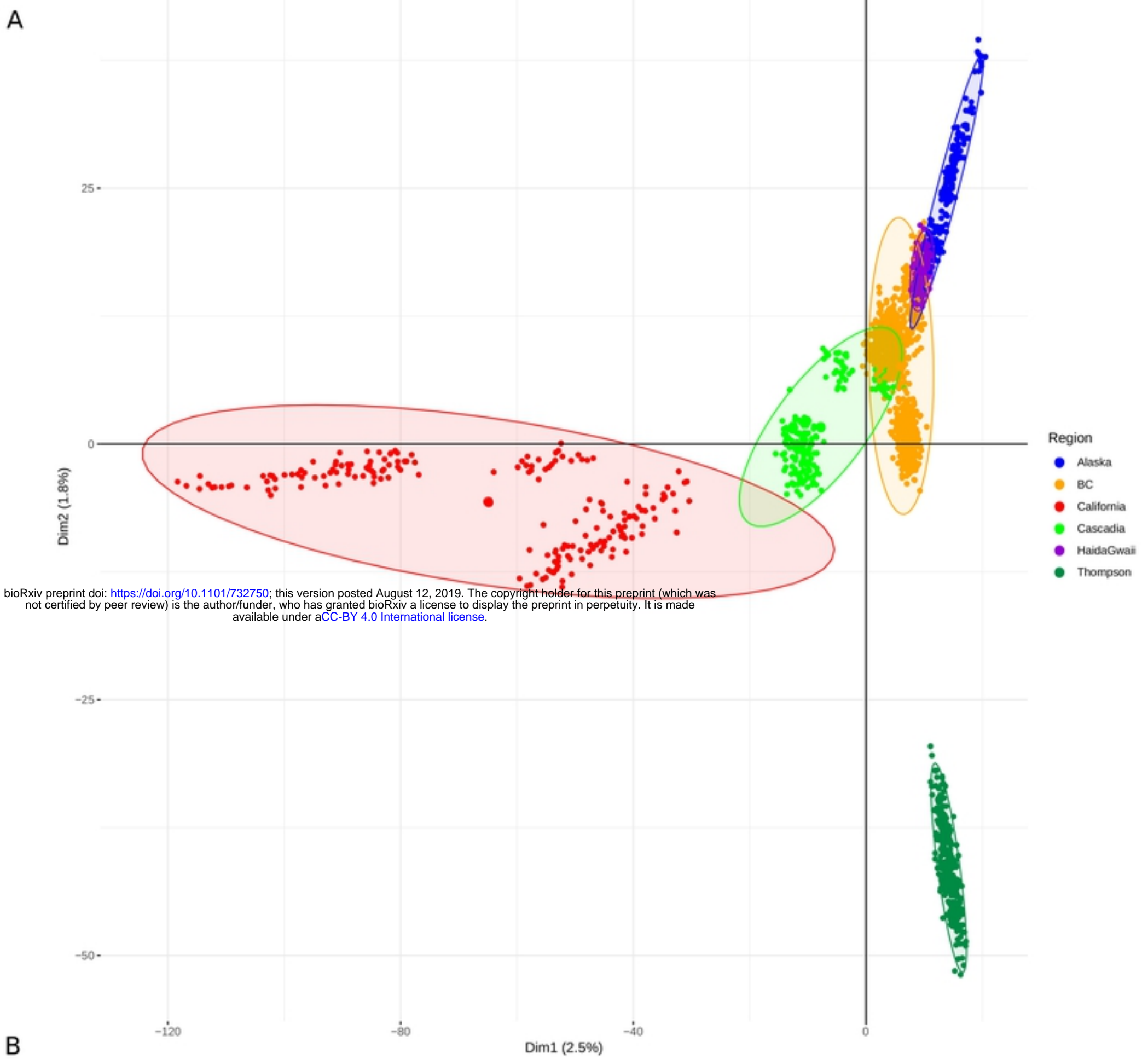


Fig 3

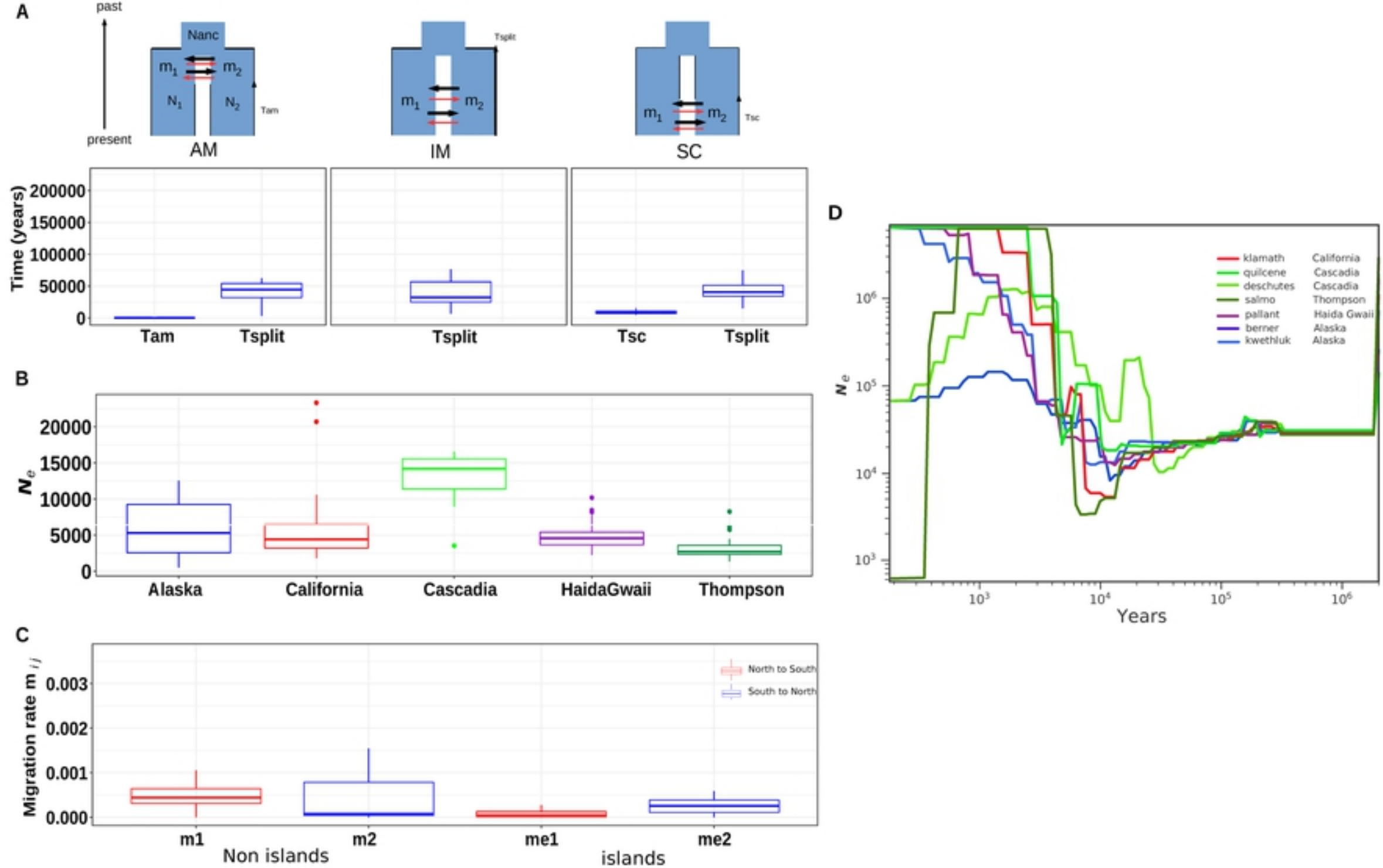


Fig 4

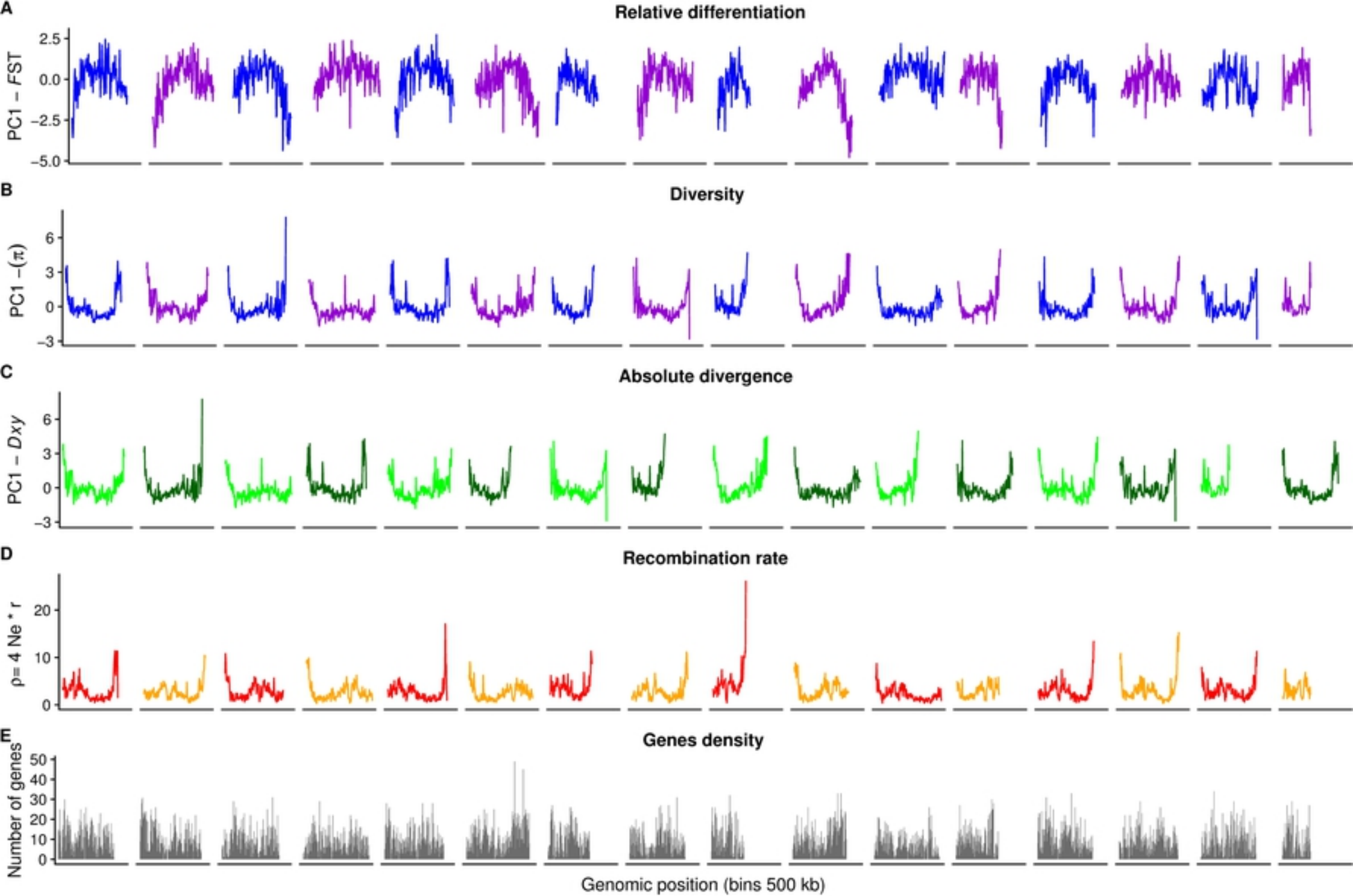


Fig 5

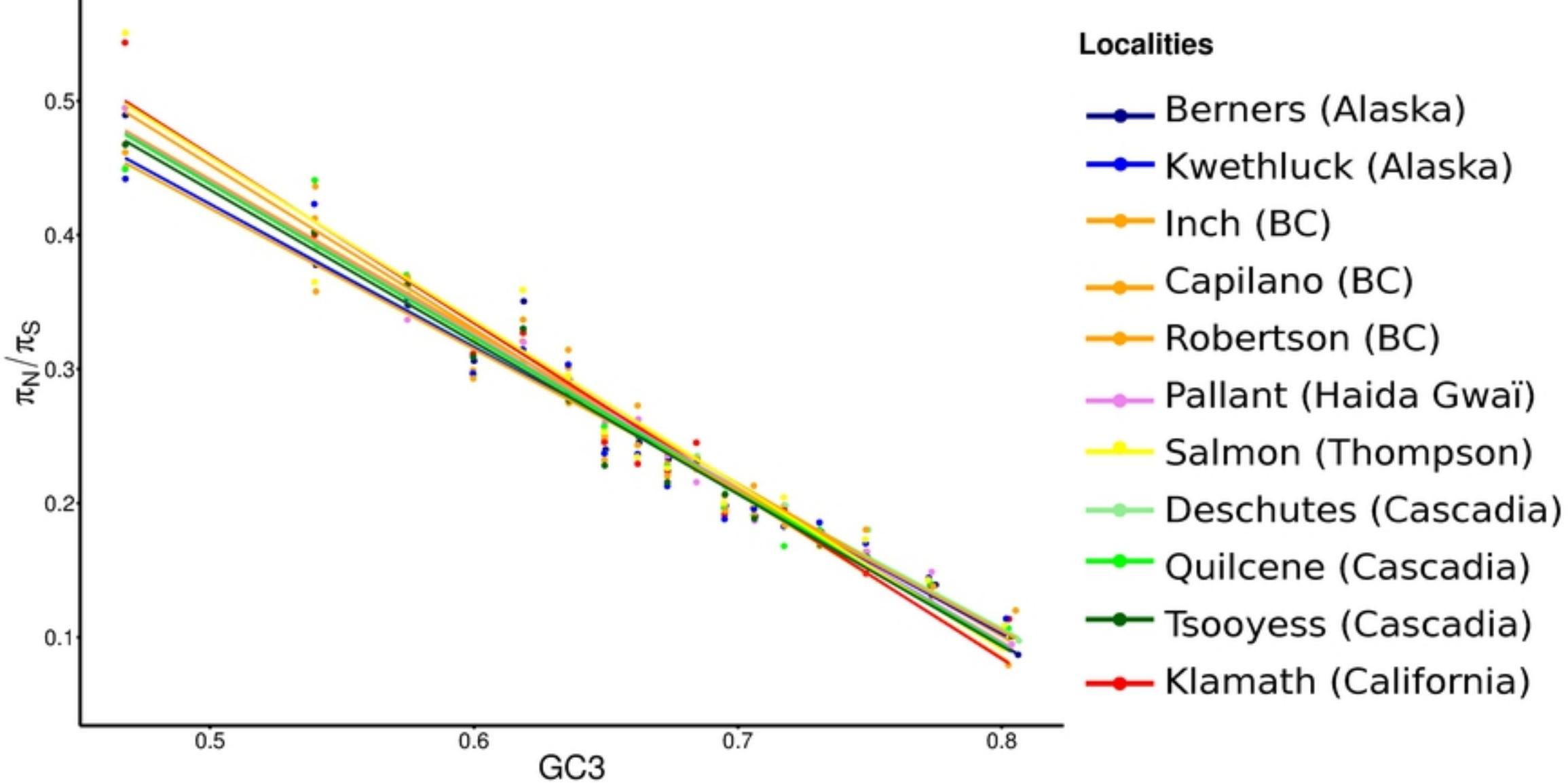


Fig 7

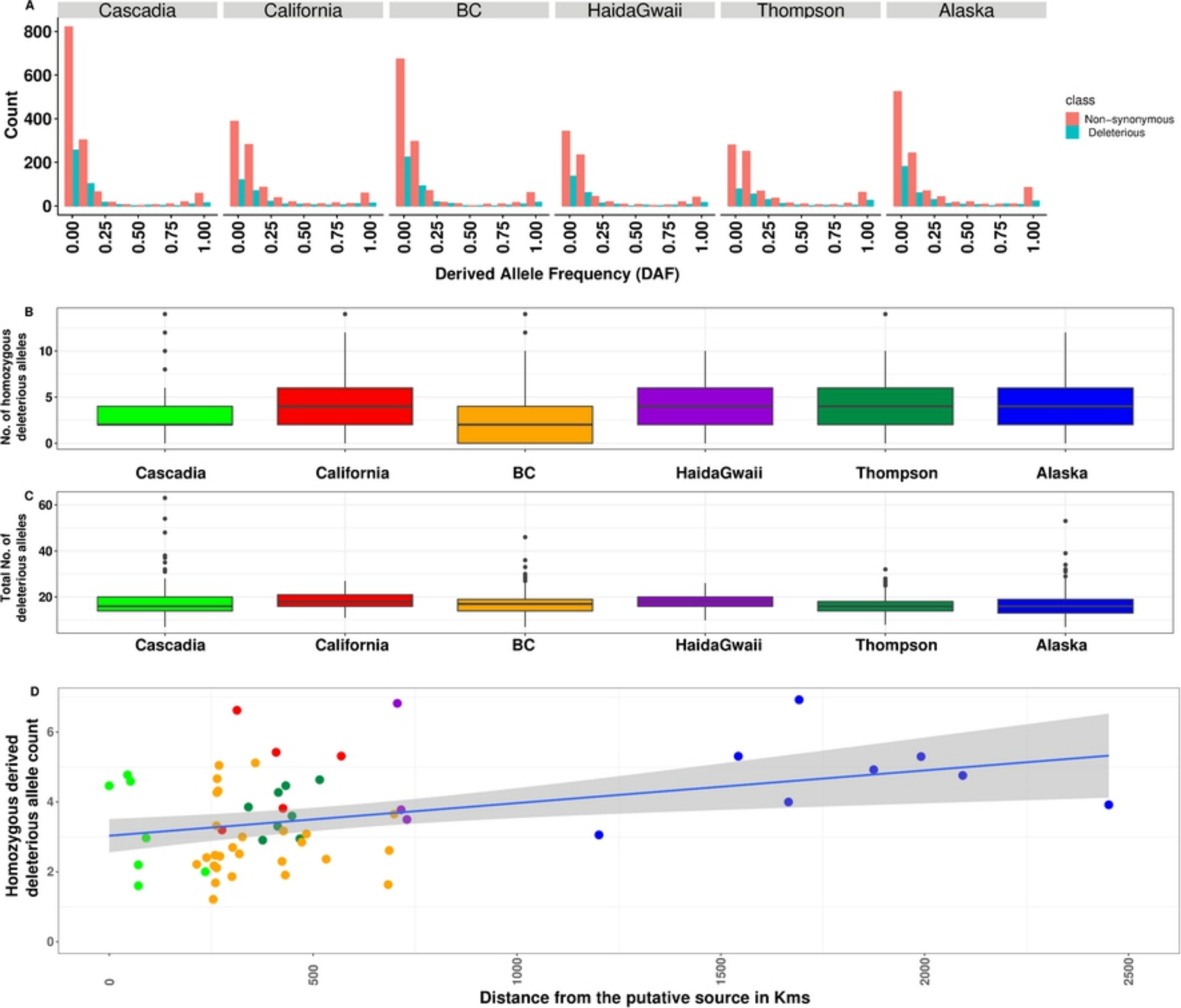


Fig 8